

Discovery of High-Affinity Inhibitors of the BPTF Bromodomain

Published as part of the Journal of Medicinal Chemistry special issue "Epigenetics 2022".

Tian Lu,[▽] Haibo Lu,[▽] Zhe Duan,[▽] Jun Wang, Jie Han, Senhao Xiao, HuanHuan Chen, Hao Jiang, Yu Chen, Feng Yang, Qi Li, Dongying Chen, Jin Lin, Bo Li, Hualiang Jiang, Kaixian Chen, Wenchao Lu,* Hua Lin,* and Cheng Luo*

 Cite This: *J. Med. Chem.* 2021, 64, 12075–12088

 Read Online

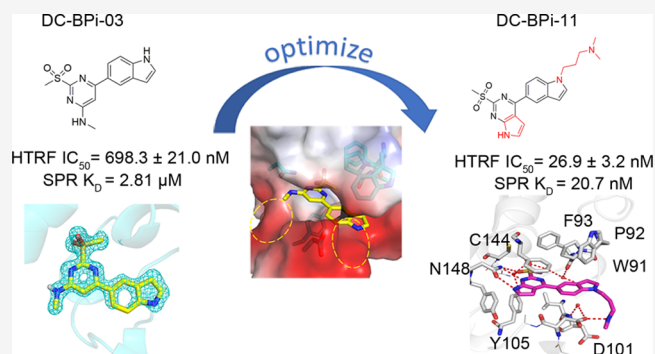
ACCESS |

 Metrics & More

 Article Recommendations

 Supporting Information

ABSTRACT: The dysfunctional bromodomain PHD finger transcription factor (BPTF) exerts a pivotal influence in the occurrence and development of many human diseases, particularly cancers. Herein, through the structural decomposition of the reported BPTF inhibitor TP-238, the effective structural fragments were synthetically modified to obtain our lead compound DC-BPi-03. DC-BPi-03 was identified as a novel BPTF-BRD inhibitor with a moderate potency ($IC_{50} = 698.3 \pm 21.0$ nM). A structure-guided structure–activity relationship exploration gave rise to two BPTF inhibitors with much higher affinities, DC-BPi-07 and DC-BPi-11. Notably, DC-BPi-07 and DC-BPi-11 show selectivities 100-fold higher than those of other BRD targets. The cocrystal structures of BPTF in complex with DC-BPi-07 and DC-BPi-11 demonstrate the rationale of chemical efforts from the atomic level. Further study showed that DC-BPi-11 significantly inhibited leukemia cell proliferation.



INTRODUCTION

Being the core subunit of the ATP-dependent nucleosome remodeling factor (NuRF) complex,¹ BPTF has 3046 amino acid residues in total, including a bromodomain and two plant homeodomain (PHD) finger domains commonly found in histone and DNA-binding proteins.² As a histone-binding component of NuRF, BPTF functionalizes the catalysis of ATP-dependent nucleosome sliding and the promotion of chromatin transcription.³ BPTF is a BRD-containing protein, which has been classified as an important research target of the non-BET family.⁴ It plays an essential role in remodeling chromatin,⁵ regulating transcription,⁶ cell differentiation,⁷ and embryogenesis.⁸

Recently, evidence showed that the dysfunction of BPTF may lead to the occurrence and development of malignant tumors,⁹ including melanoma,¹⁰ leukemia,¹¹ colorectal cancer,¹² and bladder cancer.¹³ BPTF is overexpressed in a variety of tumor tissues compared with its levels in normal tissue cells, which promotes the proliferation of cancer cells, and is an important prognostic marker in melanoma, lung cancer, and leukemia.¹⁰ BPTF can interact with *c-Myc* in oncogenic chromatin remodeling.^{5,14,15} Upon the silencing of *BPTF*, *c-Myc* transcriptional activation is completely interrupted.^{11,16} A knockdown of *BPTF* can also enhance antitumor immunity mediated by CD8⁺ T cells or NK cells.¹⁷ These previous

observations indicate that BPTF could be an important therapeutic target in cancer treatment.

So far, many effective and specific inhibitors of BET family proteins have been discovered and widely used for the treatment of various cancers.^{18–22} Meanwhile, more and more attention has been paid to the discovery and development of non-BET bromodomain inhibitors.²³ Inspiringly, the CBP/p300-BRD inhibitor CCS1477,²⁴ which was developed by Cell Centric, is the first non-BET small-molecular inhibitor that has entered clinical trials, demonstrating that targeting the non-BET family could provide more therapeutic options. Although a variety of inhibitors of BPTF-BRD have been reported (Figure 1), the discovery of selective BPTF-BRD inhibitors with high affinities is conspicuously lacking. Among them, Mishra et al. reported, in 2014 that the Plk1 inhibitor BI2536 can bind to SFW-BPTF ($K_D = 37$ μM) through the ¹⁹F NMR method.⁹ In 2015, Andrew K. Urick et al. identified the first BPTF-BRD small-molecule inhibitor that showed a

Received: April 21, 2021

Published: August 10, 2021



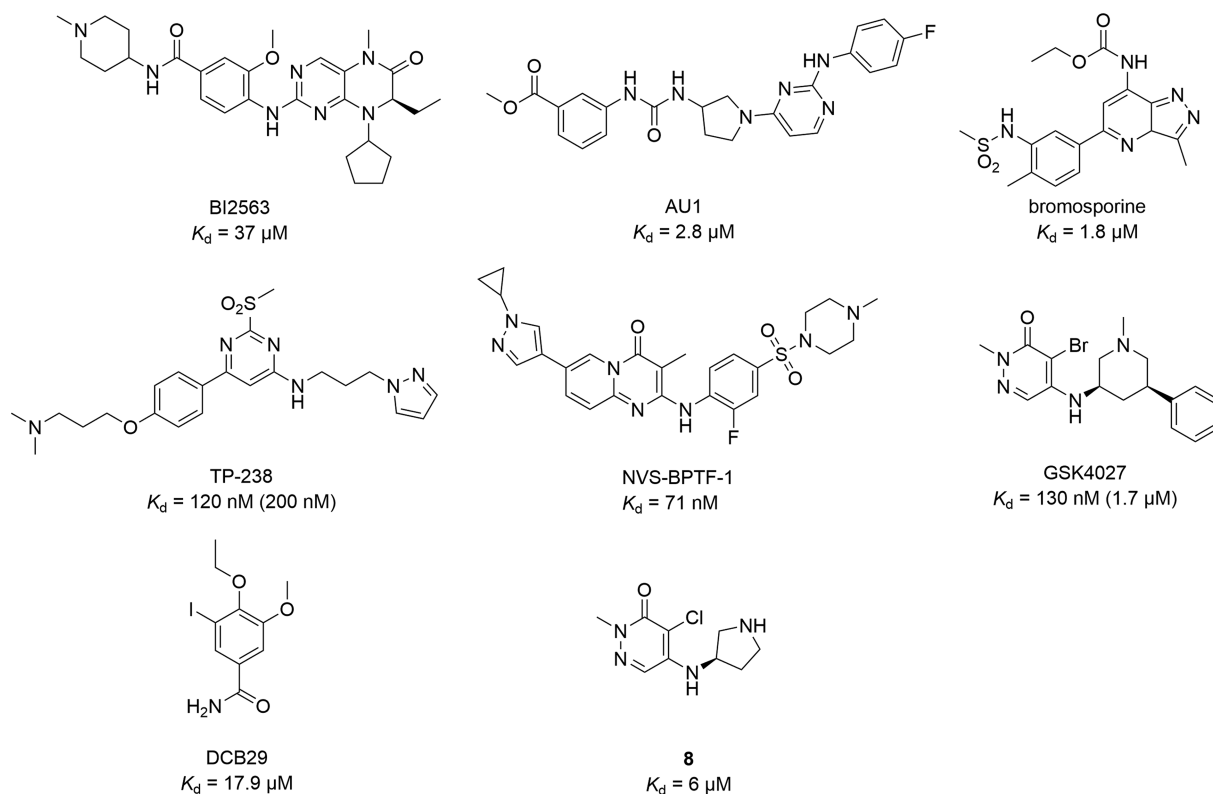


Figure 1. Representative BPTF-BRD inhibitors.

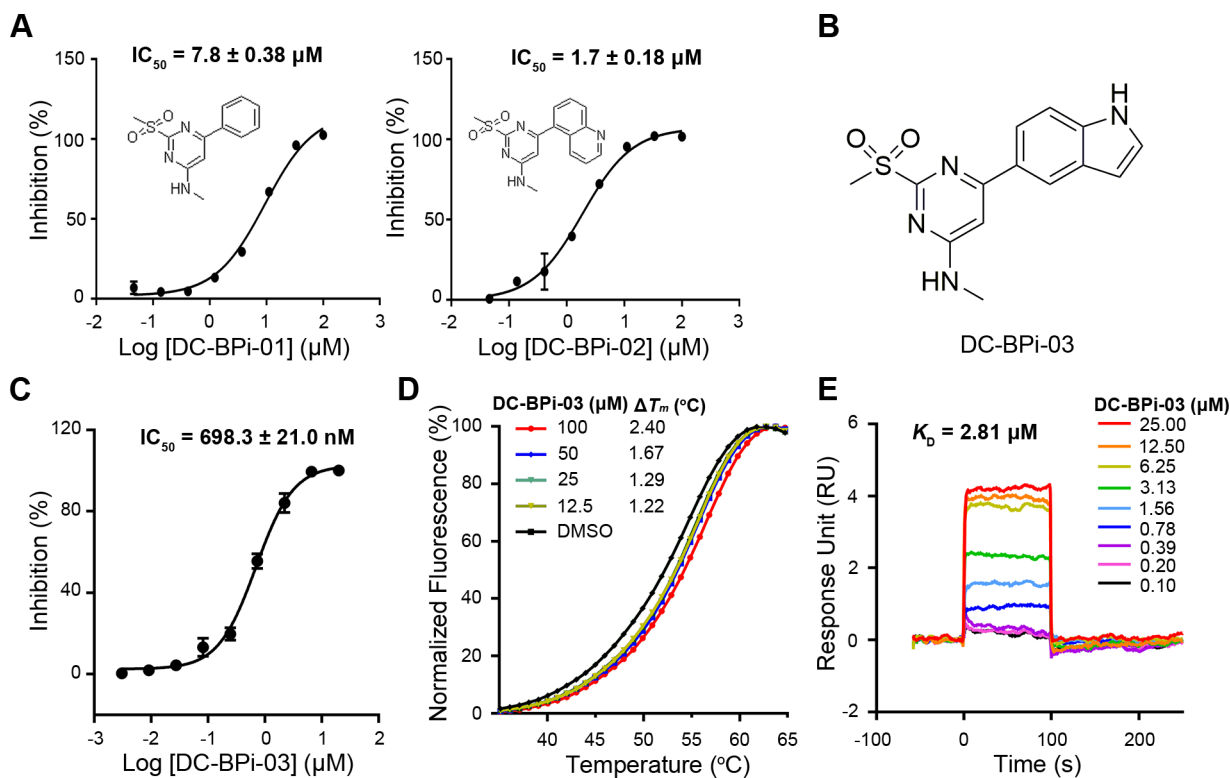


Figure 2. The discovery and preliminary validation of the hit compound DC-BPi-03. (A–C) The structures and biochemical inhibitory activities of hit compounds DC-BPi-01–DC-BPi-03. (D) The melting curves of BPTF-BRD with DC-BPi-03 at different concentrations. Fluorescence signals from protein thermal shift assays were normalized and plotted as a function of the temperature. (E) SPR assay demonstrating the binding between DC-BPi-03 and BPTF-BRD.

selectivity over BRD4, namely, AU1, using protein-observed fluorine NMR.²⁵ AU1 was further demonstrated to be active in

cells using a BPTF-specific reporter assay.²⁶ In 2016, Sarah et al. reported a broad-spectrum inhibitor, bromosporine, that

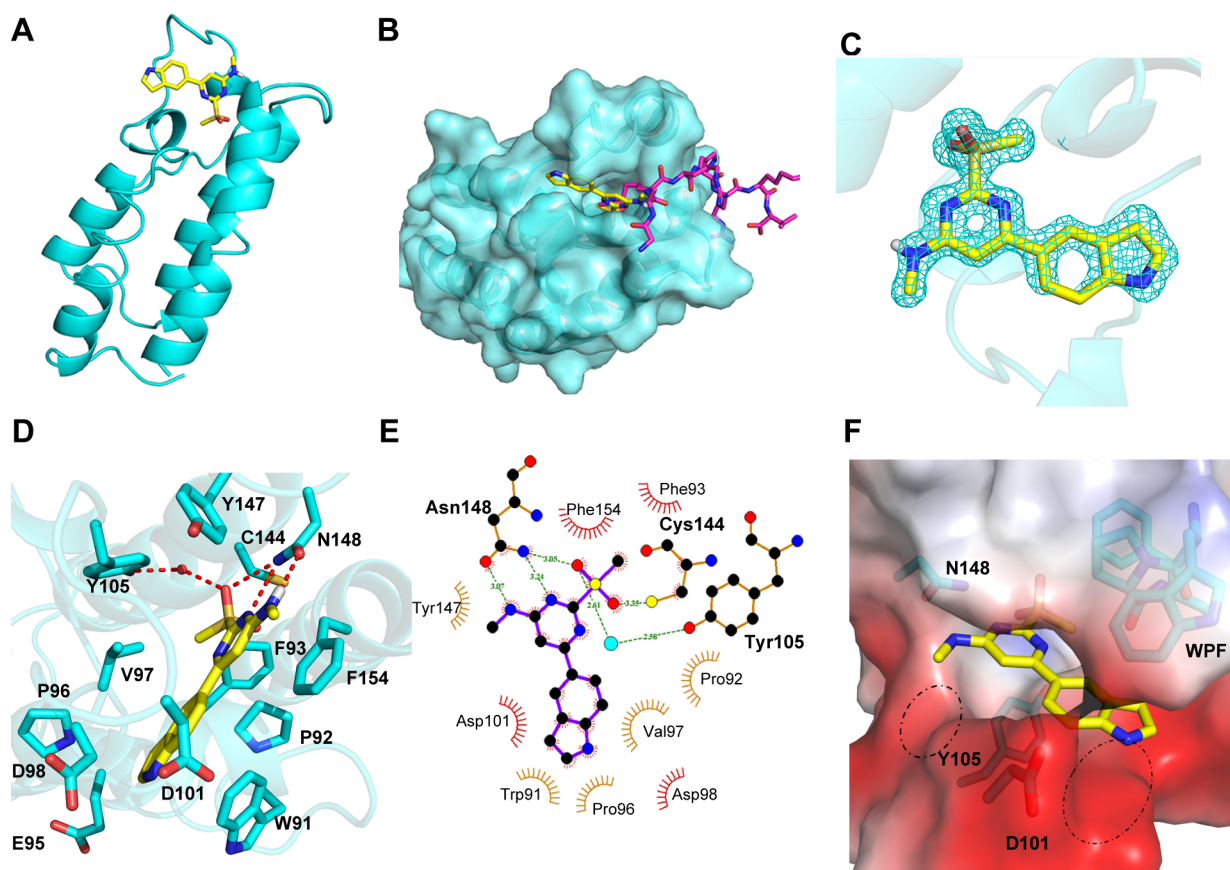


Figure 3. The cocrystal structure of BPTF-BRD with DC-BPi-03. (A) Illustration of BPTF-BRD in complex with DC-BPi-03 (PDB ID 7F5D). (B) The overlap between the acetylated H4 peptide binding pocket (PDB ID 3QZS)¹ and the DC-BPi-03 binding site. (C) The $2F_o - F_c$ electron density map for DC-BPi-03 contoured at 1.0σ . (D and E) Residues involved in BPTF and DC-BPi-03 recognition. Important residues involved in the binding between DC-BPi-03 and BPTF are shown in stick structures. (F) Potential optimization direction for DC-BPi-03.

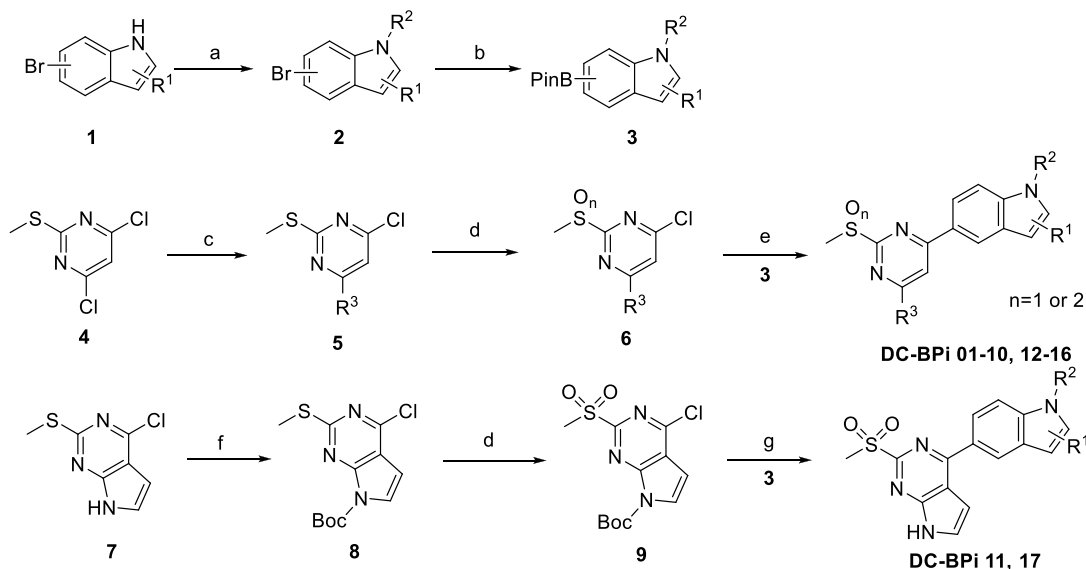
also inhibits BPTF ($K_D = 1.8 \mu\text{M}$).²⁷ In 2017, GSK discovered the PCAF and GCN5 inhibitor GSK4027. The K_i values for PCAF and GCN5 are both 1.4 nM, and it was found that GSK4027 can also bind to BPTF with a K_i value of 130 nM.²⁸ In 2018, the Structural Genomics Consortium (SGC) showed on its official website the non-peer-reviewed compound TP-238, which has a higher activity ($K_D = 120$ nM). Novartis collaborated with the SGC to develop NVS-BPTF-1 as a BPTF inhibitor with $\text{IC}_{50} = 71$ nM. Previously, by using virtual screening, our group also identified BPTF-BRD inhibitors that were alkoxy benzamide derivatives.²⁹ In 2020, the Pomerantz group reported compound **8**, which is similar in structure to GSK4027 but has an equilibrium dissociation constant (K_D) of $6.0 \pm 2 \mu\text{M}$ as determined by surface plasmon resonance technology (SPR). Additionally, the team used SPR to retest the compounds TP-238 and GSK4027, with K_D values of 200 nM and 1.7 μM , respectively.³⁰ There is a highly urgent need to discover novel BPTF inhibitors along with a cocrystal structure that may facilitate further medicinal chemistry optimization and function as chemical probes for BPTF-BRD-related biological studies.

In the present work, based on the known BPTF inhibitor TP-238 we fragmented its structure and demonstrated that its effective structural fragment is the DC-BPi-01 compound. We further modified the benzene ring structure of its side chain. The DC-BPi-02 and DC-BPi-03 compounds were modified and synthesized, and the indole structure of the DC-BPi-03 compound was more active. We selected DC-BPi-

03 as the lead compound and successfully obtained a high-resolution cocrystal structure, which provided a starting point for guiding the next step of structural modification. Through structural biology and subsequent rational medicinal chemistry design, we discovered two more potent derivatives, DC-BPi-07 and DC-BPi-11. We then successfully obtained two cocrystal structures of DC-BPi-07 and DC-BPi-11 with BPTF-BRD. Furthermore, DC-BPi-11 effectively inhibited the proliferation of human leukemia MV-4-11 cells through downregulating downstream oncogene expression while exhibiting minimal effects on normal cells, demonstrating its safety. These results indicated that this novel BPTF-BRD inhibitor is a promising molecule for further optimization and development as a therapy for BPTF-related cancers.

RESULTS AND DISCUSSION

Discovery of DC-BPi-03 through the Screening of Privileged Structural Fragments. Previously, our group applied computer-aided virtual screening to find potential BPTF inhibitors and established a stable and reproducible detection method based on HTRF for compound characterization.²⁹ Herein, we analyzed the structure of the BPTF inhibitor TP-238, which was published on the SGC Web site, and decomposed it into fragments to identify privileged substructures and motifs. The results showed that DC-BPi-01 is an effective fragment that binds to BPTF (Figure 2A). Further structural decoration led to the discovery of DC-BPi-02 and DC-BPi-03 with improved activities, among which DC-

Scheme 1. Synthesis of BPTF Compounds^a

^aReaction conditions are as follows: (a) halide, NaH, DMF, 0 °C–80 °C; (b) B₂Pin₂, KOAc, Pd(dppf)Cl₂, 1,4-dioxane, 90 °C; (c) amine, Et₃N, DMSO, 60 °C; (d) *m*-CPBA, DCM, 0 °C to rt; (e) Pd(PPh₃)₄, Na₂CO₃, 1,4-dioxane/H₂O, 90 °C; (f) (Boc)₂O, NaH, THF, 0 °C to rt; (g) Pd(dppf)Cl₂, K₃PO₄, 1,4-dioxane/H₂O, 90 °C.

BPi-03 with an indole scaffold showed an optimal inhibitory activity with an IC₅₀ value of 698.3 ± 21.0 nM (Figure 2B and C). To further confirm the binding between BPTF-BRD and DC-BPi-03, we next carried out protein thermal shift assays. Compared to that of the DMSO control, the melting temperature of BPTF-BRD evidently increased upon the addition of DC-BPi-03, indicating that the ligand may interact with BPTF-BRD and strengthen its thermal stability *in vitro* (Figure 2D).

We also used SPR to confirm the binding between DC-BPi-03 and BPTF-BRD. DC-BPi-03 directly bound to BPTF-BRD with a K_D value of 2.8 μM, which was consistent with *in vitro* HTRF data (Figure 2E). These results suggested DC-BPi-03 indeed binds to BPTF-BRD *in vitro*.

Cocrystal Structure Determination. To explore the molecular basis of the inhibitory activity of DC-BPi-03 against BPTF-BRD for further chemistry optimization, we obtained high-resolution cocrystal structures of BPTF-BRD with DC-BPi-03 at 1.58 Å to illustrate the structural basis for the binding of BPTF-BRD with DC-BPi-03 (PDB ID 7F5D). The result showed the very complete electron density of DC-BPi-03 in the substrate pocket (Figure 3A–C). DC-BPi-03 fit well within the histone binding pocket of BPTF-BRD and formed various hydrogen bonds and hydrophobic interactions with neighboring residues (Figure 3D). The sulfonyl group and the *N*-methylpiperidine group formed tridentate hydrogen bonds with the primary amide group of residue N148, which was previously found to be a crucial residue in the recognition of acetylated lysine.²⁰ DC-BPi-03 also formed a pair of water-bridged hydrogen bonds with Y105, indicating the important role of structural water within the binding pocket. In addition, DC-BPi-03 formed a variety of hydrophobic interactions with adjacent residues in the crystal structure, including W91, P92, F93, V97, Y147, and F154, through the *N*-methylpiperidine group and the cyclopentyl group (Figure 3E). These interactions were the dominant driven forces for the binding between BPTF and DC-BPi-03.

Chemistry and Structure–Activity Relationship

Study. Guided by the cocrystal structure in hand, we designed and synthesized a series of derivatives (Scheme 1). Commercially available 5-bromo indole or 6-bromo indole 1 was alkylated by the corresponding halide in the presence of NaH to provide *N*-alkyl products 2, which were coupled with B₂Pin₂ to give rise to intermediate 3. Commercially available pyrimidine 4 was reacted with the corresponding amines, following oxidation by *m*-CPBA, to afford methylsulfonyl or methylsulfinyl products 6. The coupling of 3 and 6 gave DC-BPi-1–10 and DC-BPi-12–16 in moderate yields. Commercially available 7*H*-pyrrolo[2,3-*d*]pyrimidine 7 was Boc protected before being oxidated to its corresponding methylsulfonyl intermediate 9. Then, the intermediate 9 was coupled with 3 to form DC-BPi-11 and DC-BPi-17.

According to the cocrystal structure of DC-BPi-03 and the BPTF protein, there was a negatively charged channel below the indole group and an extra pocket near the pyrimidin-4-amine group (Figure 3F). Thus, the incorporation of an alkylamine substitution to the indole nitrogen group might introduce new hydrogen bonds. Both *N,N*-dimethyl ethyl amine and propyl amine exhibited a 20-fold increase of their activities (DC-BPi-04 and DC-BPi-05, respectively). These results suggested that a new hydrogen bonding interaction was formed, which enhanced the binding affinity. Prolonging of the alkyl substitution at the pyrimidin-4-amine group in the bottom part might benefit hydrophobic interactions between the alkyl group and surrounding residues. An ethyl or propyl substituent showed more potency (DC-BPi-06 or DC-BPi-07, respectively). However, the *n*-butyl substituent was too long for the activity (DC-BPi-08). The branched alkyl group was too bulky (DC-BPi-09), which decreased the activity. The free NH of the pyrimidine ring was critical for the potency due to it forming a hydrogen bond with residue N148. Thus, it is rational to find the *N,N*-dimethyl group substituent diminished the activity (DC-BPi-10). Interestingly, 7*H*-pyrrolo[2,3-*d*]pyrimidine was well tolerated with an IC₅₀ value at 26.9 ± 3.2 nM (DC-BPi-11). Mono-oxidated compounds exhibited less

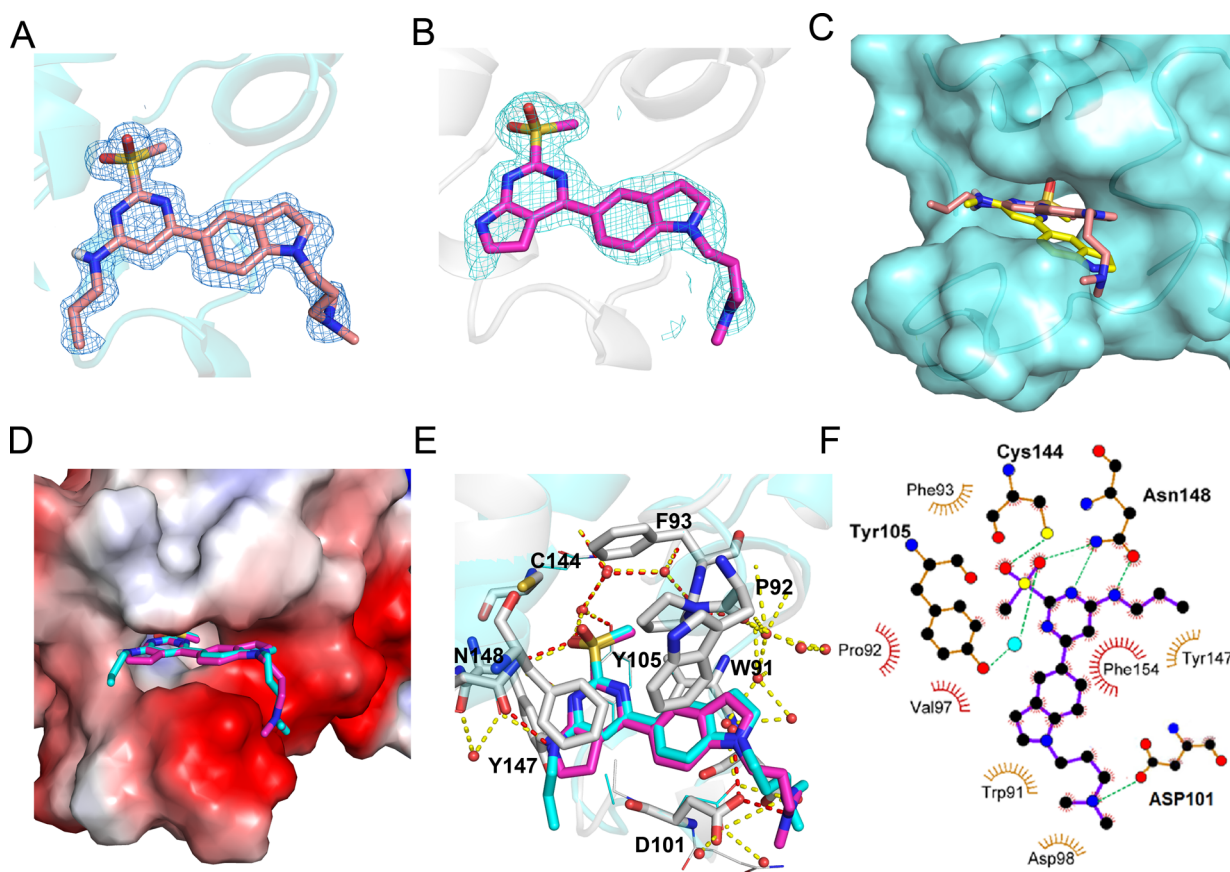


Figure 4. The cocystal structures of DC-BPi-07 and DC-BPi-11 with BPTF-BRD. (A and B) Crystal structures of BPTF-BRD with DC-BPi-07 (PDB ID 7F5C) and DC-BPi-11 (PDB ID 7F5E). The $2F_o - F_c$ electron density maps of DC-BPi-07 and DC-BPi-11 are contoured at 1.0σ . (C) The alignment of the binding conformation of DC-BPi-03 with DC-BPi-07. DC-BPi-03 and DC-BPi-07 are depicted as yellow and salmon sticks, respectively. (D) The binding pocket of BPTF for DC-BPi-07 and DC-BPi-11. (E) Residues involved in BPTF inhibitor recognition. (F) The cocystal structure of DC-BPi-07 and BPTF-BRD (PDB ID 7F5C) shows important hydrogen bonding and hydrophobic interactions between the ligand and the receptor.

potency in two cases (DC-BPi-12 and DC-BPi-13). A 60-fold potency loss occurred when the pyrimidine moiety was moved from the 6 position to the 5 position of indole ring (DC-BPi-14). It suggested the loss of a hydrogen bond interaction due to a mismatched conformation. Little negative effect was observed when a different substituent was installed to the indole ring or the 3 or 7 positions (DC-BPi-15–17, respectively). These results indicated that the indole ring could tolerate some substituents.

Cocystal Structure of BPTF in Complex with Compounds. To further clarify the molecular basis of the improved activities of DC-BPi-07 and DC-BPi-11, we successfully cocrystallized the BPTF with DC-BPi-07 and DC-BPi-11 (Figure 4A and B, respectively, PDB IDs 7F5C and 7F5E, and Tables S2 and S3). DC-BPi-07 and DC-BPi-11 were inserted deeply into the pocket and occupied the negatively charged binding site of the acetylated H4 peptide with slight conformation changes comparing with DC-BPi-03 (Figure 4C and D, respectively). DC-BPi-07 formed direct and water-bridged hydrogen bonds and hydrophobic contacts with surrounding residues within the binding pocket of the BPTF bromodomain, as DC-BPi-03 did (Figure 4D). Direct hydrogen bonds were observed between DC-BPi-07 and DC-BPi-11 and N148 and C144, while water-bridged hydrogen bonds were formed with Y105 (Figure 4E and F). As expected, the free NH of the pyrimidine moiety of DC-BPi-07 and DC-

BPi-11 formed an important hydrogen bond interaction with the aspartic acid carbonyl group of N148. Importantly, another hydrogen bond was found between the *N,N*-dimethyl alkylamine group of DC-BPi-07 and DC-BPi-11 with D101. The conformation of W91 was slightly shifted due to the better occupancy of DC-BPi-07, demonstrating the rationale of chemical efforts on the indole group (Figure 4E). In addition to polar interactions, DC-BPi-07 and DC-BPi-11 formed hydrophobic interactions with residues P92, V97, Y105, and F154. When the hydrogen on the free NH of the pyrimidine part of the compound is replaced, the activity is greatly reduced, such as for DC-BPi-10.

Biophysical Binding Assays. Table 1 and Figure S1 summarized the structures and their inhibitory activities on BPTF-H4. Among them, the derivatives DC-BPi-07 and DC-BPi-11 had the best inhibitory activities, with IC_{50} values of 16.0 ± 5.0 and 26.9 ± 3.2 nM, respectively (Figure 5A and D, respectively). To investigate interactions between DC-BPi-07, DC-BPi-11, and the BPTF bromodomain, a protein thermal shift assay was similarly carried out. As the concentrations of DC-BPi-07 and DC-BPi-11 increased, the thermostability of BPTF-BRD also increased accordingly (Figure 5B and E, respectively). Besides, in SPR assays DC-BPi-07 and DC-BPi-11 showed equilibrium dissociation constant (K_D) values of 49.6 and 20.7 nM, respectively. The values were consistent with their inhibitory activities in the HTRF assays (Figure 5C

Table 1. Chemical Modifications on DC-BPi-03

Compound ID	Structure	IC ₅₀ (nM)	Compound ID	Structure	IC ₅₀ (nM)
DC-BPi-01		7,800 ± 400	DC-BPi-10		14,700 ± 1,600
DC-BPi-02		1,700 ± 200	DC-BPi-11		26.9 ± 3.2
DC-BPi-03		698.3 ± 21.0	DC-BPi-12		59.3 ± 3.0
DC-BPi-04		32.7 ± 1.4	DC-BPi-13		145.4 ± 27.0
DC-BPi-05		36.9 ± 3.3	DC-BPi-14		2,100 ± 200
DC-BPi-06		28.8 ± 3.6	DC-BPi-15		63.8 ± 8.0
DC-BPi-07		16.0 ± 5.0	DC-BPi-16		58.6 ± 2.2
DC-BPi-08		113.8 ± 8.1	DC-BPi-17		157.3 ± 10.2
DC-BPi-09		287.6 ± 12.3			

and F). To confirm the binding between DC-BPi-11 and BPTF, both Carr–Purcell–Meiboom–Gill (CPMG) and saturation transfer difference (STD) NMR experiments were performed. As shown in Figure S2, a strong signal in the STD NMR experiment and a significantly decreased signal in the CPMG spectrum were detected under the conditions of 5 μM BPTF and 200 μM DC-BPi-11, indicating the mutual binding between BPTF-BRD and the compound. Collectively, these biophysical evidence prove that DC-BPi-11 bound to the BPTF bromodomain *in vitro*.

Selectivity Profiling. The selectivity of our compounds over the BRDs family *in vitro* was further profiled, considering that the structures of bromodomains in BRD families are highly conserved.²⁹ We tested the inhibitory activities of DC-BPi-11 using AlphaScreen against BRD4(1), BRD4(2), BRD2(1), BRD2(2), CBP-BRD, P300-BRD and SMARCA2-

BRD at a concentration of 1 μM . DC-BPi-11 exhibited complete inhibition against BPTF-BRD, while it displayed minimal activity against the other bromodomains (Figure S5G). The selectivity was also validated using protein thermal shift assays. The shift of the T_m value of BPTF-BRD with the DC-BPi-11 treatment was 8.0 $^{\circ}\text{C}$, while the T_m shift was relatively much smaller for other bromodomain targets (Figure S5H). In summary, DC-BPi-11 is the effective BPTF inhibitor, which is a promising starting point for structural optimization in the future.

We then aligned the available crystal structures of different BRDs to BPTF-DC-BPi-11 to investigate the molecular basis of the selectivity (Figure S3). We found that the aspartic acid residue D101 in BPTF that formed the hydrogen bond with the positively charged *N,N*-dimethyl alkylamine group of DC-BPi-11 was replaced by the conservative leucine in all other

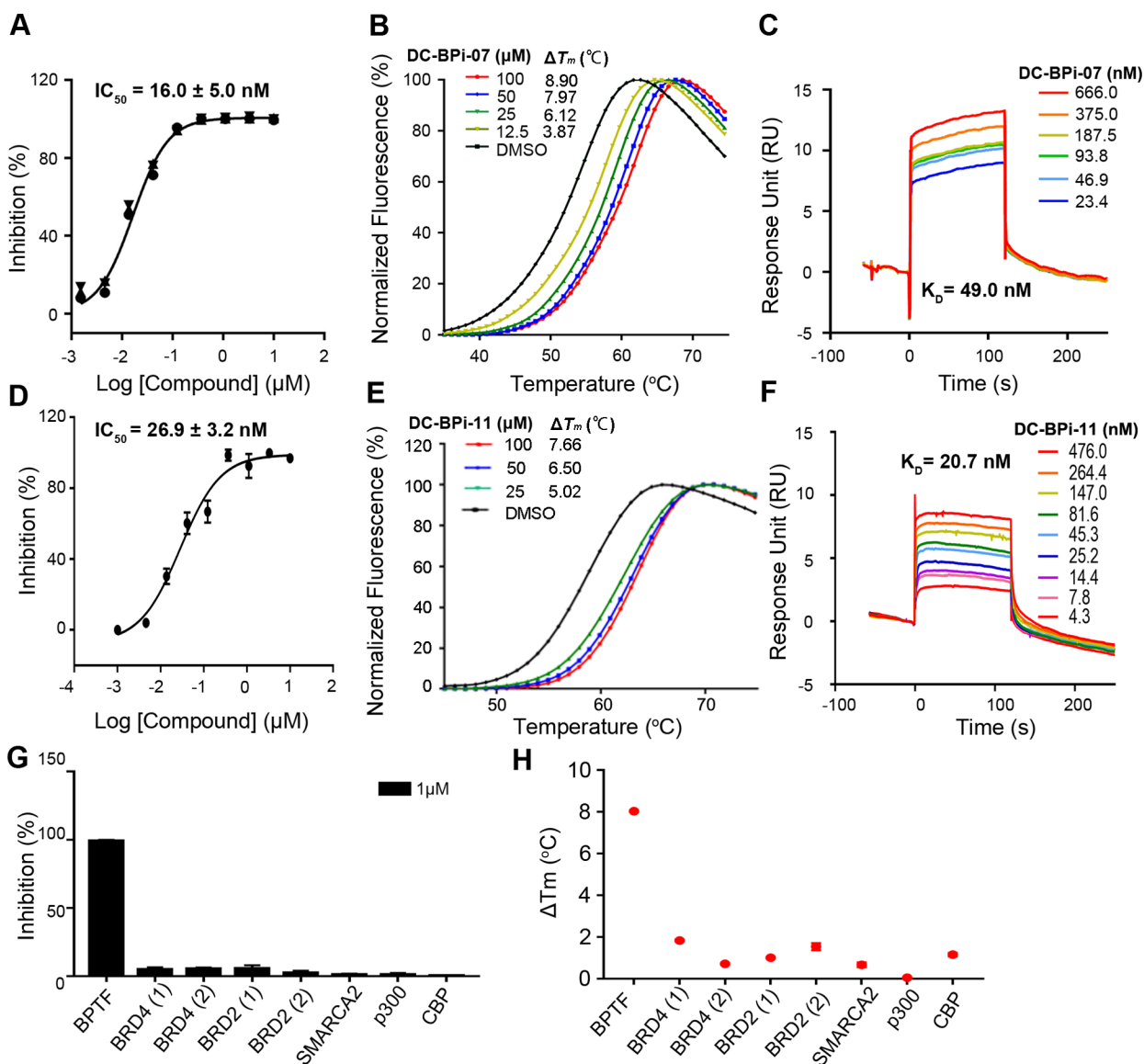


Figure 5. Biochemical and biophysical methods demonstrated the direct binding between DC-BPi-07 and DC-BPi-11 and BPTF-BRD. (A) Inhibitory activity of DC-BPi-07 against BPTF-BRD. (B) Changes in the thermodynamic stability of BPTF-BRD upon binding of DC-BPi-07. (C) SPR assay of DC-BPi-07. (D) Inhibitory activity of DC-BPi-11 against BPTF-BRD. (E) Changes in the thermodynamic stability of BPTF-BRD upon binding of DC-BPi-11. (F) SPR assay of DC-BPi-11. (G) *In vitro* inhibitory activity of compound DC-BPi-11 against BRD proteins. (H) The thermal stability effect of DC-BPi-11 on BRD proteins. The concentration of proteins was 5 μ M, and the concentration of the compound was 50 μ M.

bromodomains. Additionally, the hydrophobic residue F154 of BPTF-BRD was replaced with the valine residue in other BRDs, demonstrating the importance of the π - π stacking effect in specific recognition of DC-BPi-11.

Cell-Based Activity. To demonstrate that the identified BPTF inhibitor could directly engage the target in cells, we developed a NanoBRET assay to quantify the binding of the histone H4-HaloTag to the NanoLuc-tagged BPTF-BRD. The EC_{50} value of DC-BPi-11 is 120 nM, which also demonstrates its good target engagement and cell permeability (Figure 6A).

Previous evidence demonstrated that the knockdown of BPTF leads to impaired activation of the *c-Myc* signal in human foreskin fibroblasts.¹⁴ Numerous clinical sample analysis also indicated the higher expression level and mutation rate in melanoma and leukemia cell lines.^{10,31,32} Thus, we further explored the therapeutic potential of DC-BPi-03 and its

derivatives. Considering that BPTF is a key cofactor for *c-Myc* transcriptional activity, the well-characterized undruggable oncogene is essential for the progression of a variety of malignant diseases.¹⁴ As shown in Figure 6B, DC-BPi-11 demonstrated a potent antiproliferative effect in MV-4-11 leukemia cells, with a concentration-dependent inhibitory activity of 0.89 μ M. Meanwhile, two normal human endothelial cell lines HUV-EC-C and MRC-5 were also tested. After three days of treatment, the proliferation rate was measured using the CellTiter-Glo assay. Notably, the results showed that DC-BPi-11 had almost no inhibitory effect on the growth of normal cells even at 100 μ M (Figure S4). The downregulation of *c-Myc* was confirmed by Western blotting (Figure 6C). These results indicated that the antiproliferative effect of our compounds was, at least in part, due to the inhibition of BPTF in leukemia cell lines. Based on these data, DC-BPi-11

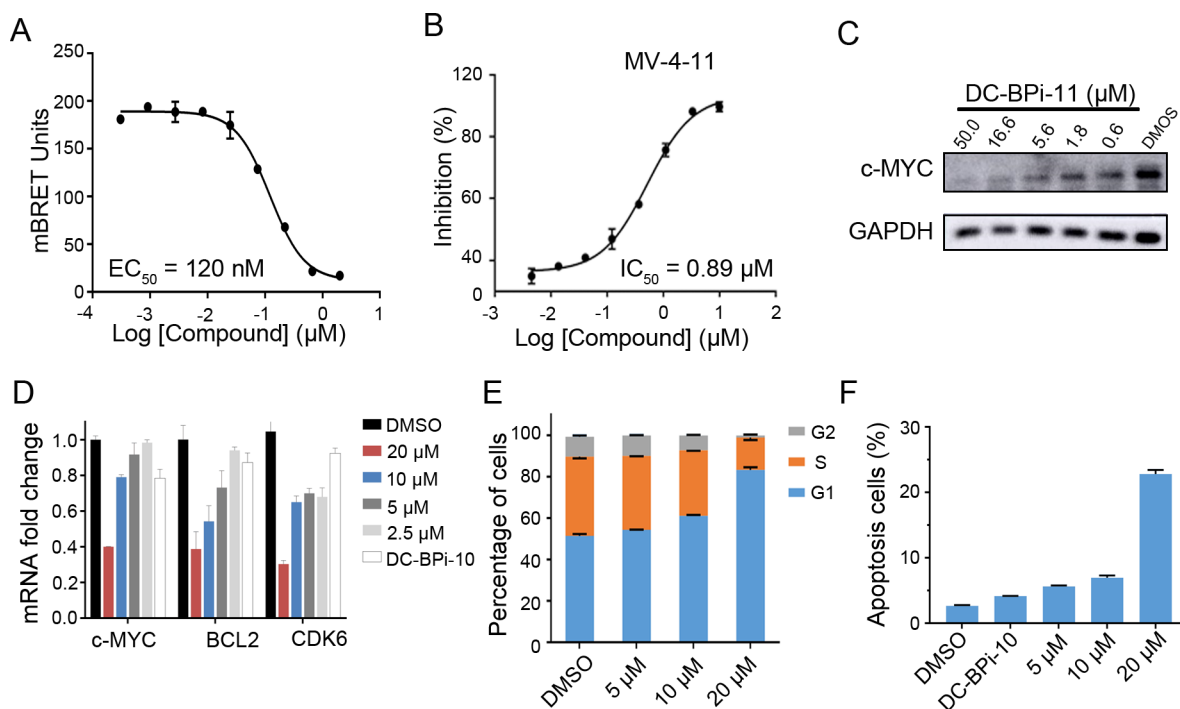


Figure 6. Cellular effect of DC-BPi-11 in MV-4-11 leukemia cells. (A) The intracellular NanoBRET experiment verifies the inhibitory effect of DC-BPi-11 on BPTF. (B) Compound effect on the proliferation of MV-4-11 cancer cells. (C) Depletion of *c-Myc* in a dose-dependent manner after compound treatment for 24 h. (D) Inhibition of the transcription of BPTF downstream genes after DC-BPi-11 treatment for 24 h at the different concentrations. (E and F) Cell cycle arrest and apoptosis were detected by flow cytometry after treatment with DC-BPi-11 for 24 h in MV-4-11 cells.

and its derivatives could be applied as promising therapeutic small molecules for the treatment of leukemia via targeting the *BPTF-Myc* axis.

Downregulation of the Expression of BPTF Target Genes. BPTF plays a crucial role in the transcriptional regulation of several oncogenes, including *c-Myc*,¹⁴ *Bcl-2*, and *CDK6*.¹⁰ Thus, RT-PCR experiments were performed to evaluate the effect of DC-BPi-11 on target gene expression at the transcriptional level. Remarkable dose-dependent decreases in the expression of target genes were observed at the mRNA level, including that of *c-Myc*, *Bcl2*, and *CDK6* (Figure 6D).

Cell Cycle and Apoptosis. Emerging evidence demonstrated that the silencing of BPTF will effectively arrest the cell cycle at the G1 phase and shorten the S phase in melanoma and mouse embryonic fibroblasts (MEFs).^{2,14} Thus, we tried to further explore if DC-BPi-11 could affect the cell cycle in MV-4-11 cells.³³ When treated with DC-BPi-11 for 24 h, a fraction of MV-4-11 cells were arrested in the G1 or S phase in a dose-dependent manner, which is consistent with genetic studies (Figure 6E).¹⁴ To determine the cell-killing effect of DC-BPi-11, we further investigated the effect of DC-BPi-11 on apoptosis. After treatment with DC-BPi-11, cells were stained with Annexin V FITC and PI, and apoptotic levels were measured using flow cytometry. Treatment with DC-BPi-11 for 24 h could significantly induce apoptosis in MV-4-11 leukemia cells (Figure 6F).

CONCLUSION

The close correlation between BPTF dysfunction and proto-oncogene signaling activation in human tumorigenesis suggests that a multitude of tumors may be affected by the therapeutic disruption of the BPTF-Myc axis. Although the pathogenesis

mechanism of oncogenes such as *c-Myc* has been investigated thoroughly, it has long been considered untargetable. Bromodomain inhibitors now make it possible to target *c-Myc* indirectly to treat tumors. Many BET inhibitors have shown an impressive efficacy in preclinical and clinical studies. However, an exploration of novel small-molecule inhibitors targeting BPTF-Myc axis is particularly lacking.

Herein, the discovery and optimization of high-affinity and selective BPTF-BRD inhibitors have been described. Through structural decomposition, we identified the privileged fragment DC-BPi-03 that could bind to BPTF. A variety of biochemical and crystallographic evidence demonstrated the binding between BPTF-BRD and DC-BPi-03. Through a combination of crystal structure analysis and rational chemical optimization, we increased the potency of BPTF-BRD inhibitors by more than 40–26-fold, resulting in the highly potent compounds DC-BPi-07 and DC-BPi-11. Based on the high-resolution crystal structure, DC-BPi-07 and DC-BPi-11 occupy the hydrophobic groove in the substrate pocket. The optimal compound in this study, DC-BPi-11, is a potent inhibitor of BPTF-BRD ($K_D = 20.7$ nM) and is selective over the other BRD family members screened. In the cell model of MV-4-11 leukemia cells, DC-BPi-11 reduced proliferation, blocked the cell cycle, and induced apoptosis, which is consistent with previous observations in BPTF genetic studies.³⁴ DC-BPi-11 is expected to enable the further deeper investigation of the role of BPTF-BRD in transcriptional regulation through chemical-genetic dissection. DC-BPi-11 could also serve to validate the potential of BPTF-BRD inhibitors in the treatment of cancers related to *c-Myc* transcription and could serve as a starting point for developing more bioavailable clinical candidates.

■ EXPERIMENTAL PROCEDURES

Chemistry. All solvents and chemicals were of reagent grade. Unless otherwise mentioned, all reagents and solvents were purchased from commercial vendors and used as received. Flash column chromatography was carried out on a Teledyne ISCO CombiFlash Rf system using prepacked columns. Solvents used include petroleum ether (PE), ethyl acetate (EtOAc; EA), dichloromethane (DCM), and methanol. The purity and characterization of compounds were established by a combination of HPLC, thin-layer chromatography (TLC), mass spectrometry, and NMR analyses. ^1H and ^{13}C NMR spectra were recorded on a Bruker AVANCE DPX-400 (400 MHz) spectrometer, a Bruker UltraShield 500 Plus spectrometer, and an AVANCE III 600 (600 MHz) spectrometer and were determined in chloroform-*d* or methanol-*d*₄ with solvent peaks as the internal reference. Chemical shifts are reported in parts per million (ppm) relative to the reference signal, and coupling constant (*J*) values are reported in hertz (Hz). TLC was performed on EMD precoated silica gel 60 F254 plates, and spots were visualized with UV light or iodine staining. Low-resolution mass spectra were recorded using a Thermo Scientific Ultimate 3000/LCQ Fleet system (ESI). High-resolution mass spectra were recorded using a Thermo Scientific EXACTIVE system (ESI). All test compounds were greater than 95% pure as determined using a Shimadzu HPLC apparatus equipped with a photodiode array detector (Kyoto, Japan). Chromatographic separation was carried out using a YMC-Triart C18 column (150 mm × 4.6 mm, 3 μm) at 35 °C. The mobile phase consisted of a 5 mM ammonium carbonate aqueous solution (eluent A) and acetonitrile (eluent B) with a gradient elution of 0–5 min 30% B, 5–15 min 30–90% B, 15–25 min 90% B, 25–27 min 90–30% B, and 27–35 min 30% B. The flow rate was 1.0 mL·min⁻¹, the injection volume was 10 μL, and the detection wavelength was set at 254 nm. Data were acquired and processed using a LabSolutions software (ver. 5.51).

General Synthesis Procedure for 2. To a solution of 1 (1 equiv) and halide (0.9 equiv) in anhydrous DMF (0.1 mM) was added NaH (2 equiv) at 0 °C. Then, the mixture was stirred at 80 °C for 3 h under a N₂ atmosphere. The reaction solution was poured into ice water. The mixture was extracted with EtOAc, washed with brine, and dried over anhydrous Na₂SO₄. The organic phase was filtered, concentrated, and purified by column chromatography to give compound 2 as the desired product.

General Synthesis Procedure for 3. To a solution of 2 (1 equiv) in anhydrous 1,4-dioxane (0.1 mM) were added B₂Pin₂ (1.2 equiv), KOAc (2 equiv), and Pd(dppf)Cl₂ (0.1 equiv). The mixture was purged with N₂ for 5 min and then stirred at 90 °C for 8 h. The reaction solution was filtered, concentrated, and purified by column chromatography to give compound 3 as the desired product.

General Synthesis Procedure for 5. To a solution of 4 (1 equiv) and amine (2 equiv) in DMSO (0.2 mM) was added Et₃N (3 equiv). The mixture was stirred at 60 °C for 6 h under a N₂ atmosphere before being diluted with EtOAc. The mixture was washed with water and brine and then dried over anhydrous Na₂SO₄. The organic phase was filtered and concentrated to use for the next step.

General Synthesis Procedure for 6. To a solution of 5 (1 equiv) in DCM (0.1 mM) was added *m*-CPBA (*n* = 1, 1 equiv; *n* = 2, 3 equiv) at 0 °C. The mixture was stirred at rt for 2 h under a N₂ atmosphere before being diluted with DCM. The mixture was washed with sodium sulfate (sat. aq.), a NaOH solution (1 M), and brine and then dried over anhydrous Na₂SO₄. The organic phase was filtered, concentrated, and purified by column chromatography to give compound 6 as the desired product.

General Synthesis Procedure for DC-BPi-01–10 and DC-BPi-12–16. To a solution of 3 (1 equiv) in 1,4-dioxane/H₂O (10:1) (0.1 mM) were added 6 (0.9 equiv), Na₂CO₃ (3 equiv), and Pd(PPh₃)₄ (0.1 equiv). The mixture was purged with N₂ and stirred at 90 °C for 12 h. The mixture was filtered and purified by column chromatography or a silica gel plate to give the desired product.

General Synthesis Procedure for 8. To a solution of 7 (1 equiv) and Boc₂O (2 equiv) in anhydrous THF (0.1 mM) was added NaH

(3 equiv) at 0 °C. The mixture was stirred at rt for 3 h under a N₂ atmosphere. The reaction solution was poured into ice water. The mixture was extracted with EtOAc, washed with brine, and dried over anhydrous Na₂SO₄. The organic phase was filtered, concentrated, and purified by column chromatography to give compound 8 as the desired product.

General Synthesis Procedure for 9. To a solution of 8 (1 equiv) in DCM (0.1 mM) was added *m*-CPBA (3 equiv) at 0 °C. The mixture was stirred at rt for 2 h under a N₂ atmosphere before being quenched with DCM. The mixture was washed with sodium sulfate (sat. aq.), a NaOH solution (1 M), and brine and then dried over anhydrous Na₂SO₄. The organic phase was filtered, concentrated, and purified by column chromatography to give compound 9 as the desired product.

General Synthesis Procedure for DC-BPi-12 and DC-BPi-16. To a solution of 9 (1 equiv) and 3 (0.9 equiv) in 1,4-dioxane/H₂O (10/1, 0.1 mM) were added K₃PO₄ (3 equiv) and Pd(dppf)Cl₂ (0.1 equiv). The mixture was purged with N₂ and stirred at 90 °C for 12 h. The mixture was filtered and purified by column chromatography or preparative TLC to give the desired product.

***N*-Methyl-2-(methylsulfonyl)-6-phenylpyrimidin-4-amine (DC-BPi-01).** Pale white solid (56 mg, 68.5% yield). ^1H NMR (400 MHz, CDCl₃, methanol-*d*₄) δ 7.93 (brs, 2H), 7.41 (brs, 3H), 6.76 (s, 1H), 6.52 (brs, 1H), 3.29 (s, 3H), 2.97 (d, *J* = 4.5 Hz, 3H). ^{13}C NMR (151 MHz, CDCl₃, methanol-*d*₄) δ 164.5, 135.8, 130.8, 128.7, 126.9, 38.7. HRMS (ESI) *m/e* calc'd for C₁₂H₁₄N₃O₂S (M + H)⁺ 264.0807, found 264.0799.

***N*-Methyl-2-(methylsulfonyl)-6-(quinolin-5-yl)pyrimidin-4-amine (DC-BPi-02).** Pale white solid (45 mg, 48.5% yield). ^1H NMR (600 MHz, methanol-*d*₄) δ 8.88 (d, *J* = 3.1 Hz, 2H), 8.71 (d, *J* = 8.5 Hz, 1H), 8.13 (d, *J* = 8.3 Hz, 1H), 7.89–7.74 (m, 2H), 7.56 (dd, *J* = 8.6, 4.2 Hz, 1H), 6.86 (d, *J* = 21.0 Hz, 1H), 3.34 (s, 2H), 3.06 (s, 3H). ^{13}C NMR (126 MHz, methanol-*d*₄) δ 165.8, 164.6, 162.6, 150.4, 147.8, 136.2, 135.1, 130.1, 129.3, 128.2, 126.3, 121.9, 108.3, 38.1, 26.8. HRMS (ESI) *m/e* calc'd for C₁₅H₁₅N₄O₂S (M + H)⁺ 315.0916, found 315.0902.

6-(1*H*-Indol-5-yl)-*N*-methyl-2-(methylsulfonyl)pyrimidin-4-amine (DC-BPi-03). Pale white solid (83 mg, 28.3% yield). ^1H NMR (600 MHz, CDCl₃, MeOD) δ 8.35 (s, 1H), 7.84 (s, 1H), 7.46 (d, *J* = 12.2 Hz, 1H), 7.29 (d, *J* = 4.8 Hz, 1H), 7.00 (s, 1H), 6.56 (d, *J* = 4.8 Hz, 1H), 3.36 (s, 3H), 3.02 (s, 3H). ^{13}C NMR (126 MHz, CDCl₃, MeOD) δ 164.6, 137.9, 128.2, 127.1, 125.8, 120.2, 119.8, 111.3, 102.4, 38.4. HRMS (ESI) *m/e* calc'd for C₁₄H₁₄N₄O₂S (M + H)⁺ 303.0916, found 303.0912.

6-(1-(3-(Dimethylamino)propyl)-1*H*-indol-5-yl)-*N*-methyl-2-(methylsulfonyl)pyrimidin-4-amine (DC-BPi-04). Pale yellow solid (65 mg, 54.1% yield). ^1H NMR (600 MHz, methanol-*d*₄) δ 8.29 (brs, 1H), 7.82 (brs, 1H), 7.43 (d, *J* = 8.4 Hz, 1H), 7.25 (d, *J* = 3.6 Hz, 1H), 6.94 (s, 1H), 6.53 (d, *J* = 2.4 Hz, 1H), 4.20 (t, *J* = 7.2 Hz, 2H), 3.34 (s, 3H), 2.97 (s, 3H), 2.38–2.36 (m, 2H), 2.27 (s, 6H), 2.04–1.99 (m, 2H). ^{13}C NMR (126 MHz, methanol-*d*₄) δ 165.5, 164.6, 162.8, 137.6, 129.1, 128.9, 127.1, 120.1, 109.3, 102.1, 101.3, 56.0, 43.8, 43.6, 37.9, 27.3, 26.6. HRMS (ESI) *m/e* calc'd for C₁₉H₂₆N₅O₂S (M + H)⁺ 388.1807, found 388.1807.

6-(1-(2-(Dimethylamino)ethyl)-1*H*-indol-5-yl)-*N*-methyl-2-(methylsulfonyl)pyrimidin-4-amine (DC-BPi-05). Pale yellow solid (41 mg, 26.7% yield). ^1H NMR (600 MHz, Chloroform-*d*) δ 8.32 (s, 1H), 7.86 (brs, 1H), 7.38 (d, *J* = 8.4 Hz, 1H), 7.19 (d, *J* = 2.4 Hz, 1H), 6.79 (s, 1H), 6.57 (brs, 1H), 5.94–5.67 (m, 1H), 4.23 (t, *J* = 6.6 Hz, 2H), 3.38 (s, 3H), 3.01 (d, *J* = 5.4 Hz, 3H), 2.71 (t, *J* = 7.1 Hz, 2H), 2.29 (s, 6H), 2.11 (brs, 2H). ^{13}C NMR (126 MHz, chloroform-*d*) δ 165.4, 164.5, 137.7, 129.4, 128.8, 127.3, 120.7, 109.5, 102.7, 58.9, 45.7, 44.8, 38.9, 28.5. HRMS (ESI) *m/e* calc'd for C₁₈H₂₄N₅O₂S (M + H)⁺ 374.1651, found 374.1647.

6-(1-(3-(Dimethylamino)propyl)-1*H*-indol-5-yl)-*N*-ethyl-2-(methylsulfonyl)pyrimidin-4-amine (DC-BPi-06). Pale yellow solid (60 mg, 48.2% yield). ^1H NMR (600 MHz, methanol-*d*₄) δ 8.30 (brs, 1H), 7.84 (brs, 1H), 7.44 (d, *J* = 8.4 Hz, 1H), 7.26 (d, *J* = 3.0 Hz, 1H), 6.95 (s, 1H), 6.53 (d, *J* = 2.4 Hz, 1H), 4.20 (t, *J* = 6.6 Hz, 1H), 3.49–3.43 (m, 2H), 3.34 (s, 2H), 2.35 (t, *J* = 7.2 Hz, 1H), 2.25 (s, 3H), 2.03–1.98 (m, 2H), 1.24 (t, *J* = 7.2 Hz, 1H). ^{13}C NMR (126

MHz, methanol- d_4) δ 165.5, 163.8, 162.9, 137.6, 129.1, 128.9, 127.2, 120.1, 120.0, 109.3, 102.0, 101.3, 56.1, 43.8, 43.6, 37.9, 35.5, 27.4, 13.3. HRMS (ESI) m/e calc'd for $C_{20}H_{28}N_5O_2S$ (M + H)⁺ 402.1964, found 402.1955.

6-(1-(3-(Dimethylamino)propyl)-1H-indol-5-yl)-2-(methylsulfonyl)-N-propylpyrimidin-4-amine (DC-BPI-07). Pale yellow solid (58 mg, 44.9% yield). ¹H NMR (600 MHz, CDCl₃) δ 8.32 (s, 1H), 7.83 (d, J = 5.4 Hz, 1H), 7.38 (d, J = 13.2 Hz, 1H), 7.15 (d, J = 4.2 Hz, 1H), 6.82 (s, 1H), 6.54 (d, J = 4.2 Hz, 1H), 5.73 (s, 1H), 4.20 (t, J = 9.6 Hz, 2H), 3.37 (s, 3H), 3.37 (brs, 1H), 2.29 (t, J = 10.2 Hz, 2H), 2.26 (s, 6H), 1.96–2.04 (m, 2H), 1.61–1.69 (m, 2H), 0.98 (t, J = 11.4 Hz, 3H). ¹³C NMR (126 MHz, CDCl₃) δ 165.6, 163.9, 137.8, 129.4, 128.8, 127.4, 120.7, 109.7, 102.6, 56.1, 45.1, 44.1, 39.0, 27.9, 22.5, 11.5. HRMS (ESI) m/e calc'd for $C_{21}H_{30}N_5O_2S$ (M + H)⁺ 416.2115, found 416.2111.

N-Butyl-6-(1-(3-(dimethylamino)propyl)-1H-indol-5-yl)-2-(methylsulfonyl)pyrimidin-4-amine (DC-BPI-08). Pale yellow solid (72 mg, 37.2% yield). ¹H NMR (600 MHz, methanol- d_4) δ 8.34 (s, 1H), 7.91 (s, 1H), 7.53 (d, J = 8.7 Hz, 1H), 7.32 (d, J = 3.1 Hz, 1H), 6.60 (d, J = 3.1 Hz, 1H), 4.32 (t, J = 7.2 Hz, 2H), 3.45 (brs, 3H), 3.35 (s, 3H), 2.79 (t, J = 7.2 Hz, 2H), 2.59 (s, 5H), 2.21–2.16 (m, 2H), 1.65 (brs, 2H), 1.46 (brs, 2H), 0.99 (t, J = 7.2 Hz, 3H). ¹³C NMR (126 MHz, CDCl₃) δ 165.5, 163.7, 137.5, 129.1, 128.8, 127.6, 120.8, 120.7, 109.6, 103.0, 55.6, 44.0, 43.6, 38.9, 31.2, 29.7, 26.5, 20.1, 13.8. HRMS (ESI) m/e calc'd for $C_{22}H_{32}N_5O_2S$ (M + H)⁺ 430.2277, found 430.2281.

N-(sec-Butyl)-6-(1-(3-(dimethylamino)propyl)-1H-indol-5-yl)-2-(methylsulfonyl)pyrimidin-4-amine (DC-BPI-09). Pale yellow solid (72 mg, 37.2% yield). ¹H NMR (600 MHz, chloroform- d) δ 8.33 (brs, 1H), 7.85 (d, J = 7.8 Hz, 1H), 7.39 (d, J = 6.0 Hz, 1H), 7.17 (brs, 1H), 6.83 (s, 1H), 6.57 (brs, 1H), 5.52 (brs, 1H), 4.22 (t, J = 7.2 Hz, 2H), 3.38 (s, 3H), 2.36 (t, J = 7.2 Hz, 2H), 2.29 (s, 6H), 2.06–2.03 (m, 2H), 1.62–1.59 (m, 2H), 1.25 (d, J = 6.6 Hz, 3H), 0.97 (t, J = 7.8 Hz, 3H). ¹³C NMR (126 MHz, CDCl₃) δ 165.6, 163.2, 137.7, 129.3, 128.8, 127.4, 120.6, 109.7, 102.6, 55.9, 48.9, 44.7, 44.1, 38.9, 29.5, 27.53, 20.0, 10.3. HRMS (ESI) m/e calc'd for $C_{22}H_{32}N_5O_2S$ (M + H)⁺ 430.2277, found 430.2269.

6-(1-(3-(Dimethylamino)propyl)-1H-indol-5-yl)-N,N-dimethyl-2-(methylsulfonyl)pyrimidin-4-amine (DC-BPI-10). Pale yellow solid (68 mg, 54.7% yield). ¹H NMR (600 MHz, CDCl₃) δ 8.36 (d, J = 1.8 Hz, 1H), 7.90 (dd, J = 9.0, 1.8 Hz, 1H), 7.43 (d, J = 8.4 Hz, 1H), 7.17 (d, J = 3.0 Hz, 1H), 6.90 (s, 1H), 6.58 (d, J = 3.0 Hz, 1H), 4.23 (t, J = 7.2 Hz, 2H), 3.39 (s, 3H), 3.24 (brs, 6H), 2.20–2.25 (m, 2H), 2.22 (s, 6H), 1.97–2.02 (m, 2H); ¹³C NMR (126 MHz, CDCl₃) δ 165.4, 164.8, 163.4, 137.8, 129.4, 128.9, 127.9, 120.8, 120.7, 109.8, 102.5, 98.6, 56.3, 45.5, 44.3, 39.0, 37.7, 28.3; HRMS (ESI) m/e calc'd for $C_{20}H_{28}N_5O_2S$ (M + H)⁺ 402.1958, found 402.1949.

N,N-Dimethyl-3-(5-(2-(methylsulfonyl)-7H-pyrrolo[2,3-*d*]pyrimidin-4-yl)-1H-indol-1-yl)propan-1-amine (DC-BPI-11). Pale yellow solid (70 mg, 58.7% yield). ¹H NMR (400 MHz, CDCl₃, MeOD) δ 8.42 (brs, 1H), 8.00 (d, J = 8.0 Hz, 1H), 7.58 (d, J = 3.6 Hz, 1H), 7.42 (d, J = 8.0 Hz, 1H), 7.12 (d, J = 3.2 Hz, 1H), 6.96 (d, J = 3.6 Hz, 1H), 6.54 (d, J = 3.2 Hz, 1H), 4.15 (t, J = 6.4 Hz, 2H), 3.37 (s, 3H), 2.21 (t, J = 6.8 Hz, 2H), 2.13 (s, 6H), 1.99–1.91 (m, 2H). ¹³C NMR (126 MHz, CDCl₃, MeOD) δ 159.4, 157.5, 151.6, 137.6, 129.8, 129.3, 128.8, 128.2, 122.9, 122.7, 116.8, 109.8, 102.7, 102.1, 56.5, 45.0, 44.3, 40.0, 27.9. HRMS (ESI) m/e calc'd for $C_{19}H_{26}N_5OS$ (M + H)⁺ 372.1651, found 372.1646.

6-(1-(3-(Dimethylamino)propyl)-1H-indol-5-yl)-N-methyl-2-(methylsulfonyl)pyrimidin-4-amine (DC-BPI-12). Pale yellow solid (44 mg, 30.4% yield). ¹H NMR (600 MHz, methanol- d_4) δ 8.36 (brs, 1H), 7.89 (brs, 1H), 7.48 (d, J = 8.4 Hz, 1H), 7.28 (d, J = 3.0 Hz, 1H), 6.89 (s, 1H), 6.56 (d, J = 3.0 Hz, 1H), 4.24 (t, J = 7.2 Hz, 2H), 3.00 (s, 3H), 2.96 (s, 3H), 2.40 (t, J = 7.2 Hz, 2H), 2.30 (s, 6H), 2.08–1.99 (m, 2H). ¹³C NMR (151 MHz, methanol- d_4) δ 159.4, 157.5, 151.6, 137.6, 129.8, 129.3, 128.8, 128.2, 122.9, 122.7, 116.8, 109.8, 102.7, 102.1, 56.5, 45.0, 44.3, 40.0, 27.9. HRMS (ESI) m/e calc'd for $C_{19}H_{26}N_5OS$ (M + H)⁺ 372.1858, found 372.1849.

6-(1-(3-(Dimethylamino)propyl)-1H-indol-5-yl)-2-(methylsulfinyl)-N-propylpyrimidin-4-amine (DC-BPI-13). Pale yellow solid (100

mg, 51.1% yield). ¹H NMR (600 MHz, methanol- d_4) δ 8.36 (s, 1H), 7.91 (d, J = 12.6 Hz, 1H), 7.51 (d, J = 12.6 Hz, 1H), 7.29 (d, J = 4.8 Hz, 1H), 6.91 (s, 1H), 6.57 (d, J = 4.8 Hz, 1H), 4.27 (t, J = 10.2 Hz, 2H), 3.45 (brs, 2H), 2.96 (s, 3H), 2.50–2.46 (m, 2H), 2.35 (s, 6H), 2.12–2.04 (m, 2H), 1.91 (s, 1H), 1.66–1.68 (m, 2H), 1.01 (t, J = 10.8 Hz, 3H). ¹³C NMR (126 MHz, CDCl₃) δ 172.6, 164.0, 137.6, 129.2, 128.8, 127.9, 120.7, 120.6, 109.6, 102.5, 56.1, 45.0, 44.1, 43.7, 40.1, 27.8, 22.5, 11.5. HRMS (ESI) m/e calc'd for $C_{21}H_{29}N_5OS$ (M + H)⁺ 400.2171, found 400.2162.

6-(1-(3-(Dimethylamino)propyl)-1H-indol-6-yl)-N-methyl-2-(methylsulfonyl)pyrimidin-4-amine (DC-BPI-14). Pale yellow solid (25 mg, 20.7% yield). ¹H NMR (400 MHz, methanol- d_4) δ 8.34 (brs, 1H), 7.65–7.63 (m, 2H), 7.40 (d, J = 2.8 Hz, 1H), 7.07 (s, 1H), 6.54 (d, J = 2.8 Hz, 1H), 4.41 (t, J = 6.8 Hz, 2H), 3.37 (s, 3H), 3.10 (t, J = 8.0 Hz, 2H), 2.10 (s, 3H), 2.81 (s, 6H), 2.34–2.26 (m, 2H). ¹³C NMR (151 MHz, methanol- d_4) δ 165.6, 164.5, 162.6, 136.1, 131.0, 130.1, 129.3, 120.7, 117.5, 108.5, 101.9, 101.6, 55.2, 48.4, 42.7, 42.3, 37.8, 25.6. HRMS (ESI) m/e calc'd for $C_{19}H_{25}N_5O_2S$ (M + H)⁺ 388.1807, found 388.1808.

6-(1-(3-(Dimethylamino)propyl)-7-methoxy-1H-indol-5-yl)-2-(methylsulfonyl)-N-propylpyrimidin-4-amine (DC-BPI-15). Pale yellow solid (80 mg, 42.7% yield). ¹H NMR (400 MHz, methanol- d_4) δ 7.88 (brs, 1H), 7.36 (brs, 1H), 7.15 (d, J = 3.2 Hz, 1H), 6.98 (s, 1H), 6.48 (d, J = 2.8 Hz, 1H), 4.45 (t, J = 6.8 Hz, 2H), 4.01 (s, 3H), 3.41 (brs, 2H), 3.34 (s, 3H), 2.728 (d, J = 7.6 Hz, 1H), 2.54 (s, 6H), 2.15–2.08 (m, 2H), 1.69–1.61 (m, 2H), 0.99 (t, J = 7.2 Hz, 3H). ¹³C NMR (126 MHz, methanol- d_4) δ 165.5, 164.0, 162.9, 147.3, 131.1, 130.0, 128.3, 127.0, 113.2, 102.5, 101.5, 100.8, 55.6, 54.7, 46.1, 43.0, 42.3, 37.8, 28.2, 22.1, 10.4. HRMS (ESI) m/e calc'd for $C_{22}H_{32}N_5O_3S$ (M + H)⁺ 446.2226, found 446.2211.

6-(1-(3-(Dimethylamino)propyl)-3-methyl-1H-indol-5-yl)-2-(methylsulfonyl)-N-propylpyrimidin-4-amine (DC-BPI-16). Pale yellow solid (87 mg, 45.9% yield). ¹H NMR (600 MHz, methanol- d_4) δ 8.21 (brs, 1H), 7.79 (brs, 1H), 7.36 (d, J = 9.0 Hz, 1H), 7.01 (s, 1H), 6.97 (brs, 1H), 4.15 (t, J = 6.6 Hz, 2H), 3.38 (brs, 2H), 3.32 (s, 3H), 3.30–3.29 (m, 1H), 2.83 (t, J = 7.8 Hz, 2H), 2.62 (s, 6H), 2.28 (s, 3H), 2.14–2.09 (m, 2H), 1.64–1.61 (m, 2H), 0.96 (t, J = 7.2 Hz, 2H). ¹³C NMR (151 MHz, methanol- d_4) δ 165.5, 163.9, 163.1, 137.9, 129.0, 126.7, 126.6, 120.2, 118.0, 111.7, 109.1, 101.3, 55.4, 42.6, 42.3, 37.9, 29.4, 25.9, 22.1, 10.5, 8.3. HRMS (ESI) m/e calc'd for $C_{22}H_{32}N_5O_2S$ (M + H)⁺ 430.2277, found 430.2272.

N,N-Dimethyl-3-(3-methyl-5-(2-(methylsulfonyl)-7H-pyrrolo[2,3-*d*]pyrimidin-4-yl)-1H-indol-1-yl)propan-1-amine (DC-BPI-17). Pale yellow solid (50 mg, 40.4% yield). ¹H NMR (400 MHz, chloroform- d) δ 8.30 (d, J = 2.0 Hz, 1H), 7.96 (dd, J = 8.8, 2.0 Hz, 1H), 7.56 (d, J = 3.6 Hz, 1H), 7.35 (d, J = 8.8 Hz, 1H), 6.94 (d, J = 3.2 Hz, 1H), 6.90 (brs, 1H), 4.12 (t, J = 6.4 Hz, 2H), 3.36 (s, 3H), 3.27 (s, 1H), 2.50 (t, J = 8.0 Hz, 2H), 2.35 (s, 6H), 2.28 (s, 3H), 2.09–2.02 (m, 2H). ¹³C NMR (151 MHz, chloroform- d) δ 159.4, 157.2, 151.4, 137.8, 130.5, 129.0, 127.4, 126.7, 122.7, 121.0, 116.8, 112.0, 109.5, 102.0, 56.3, 44.7, 43.8, 40.2, 27.6, 9.5. HRMS (ESI) m/e calc'd for $C_{21}H_{26}N_5O_2S$ (M + H)⁺ 412.1807, found 412.1798.

Protein Expression and Purification. The human BPTF bromodomain (residues 2914–3037) was expressed and purified as previously described.²⁹ Briefly, a BPTF_{2914–3037} construct containing a PreScission protease-cleavable N-terminal GST-tag was expressed in *Escherichia coli* BL21-CodonPlus (DE3) cells. For the HTRF assay, GST-BPTF_{2914–3037} fusion protein was purified in a final buffer containing 20 mM HEPES pH 8.5, 100 mM NaCl, 5% glycerol, and 1 mM DTT. The GST tag was removed by PreScission protease for further experiments, except for the HTRF assay.

HTRF Assay. The HTRF assay was developed as previously described with a minor optimization where the fluorescence was measured using an Envision plate reader (excitation of 340 nm, emission of 665 and 620 nm, and lag time of 60 μ s) according to the assay manufacturer's recommendations.²⁹

Protein Thermal Shift Assay. The protein thermal shift assay was performed in a QuantStudio 6 Flex Real-Time PCR system. Before the thermal cycle (ramped from 25 to 95 °C), 5 μ M protein was mixed with 5 \times SYPRO Orange (Sigma-Aldrich, catalog no.

S5692). All compounds were tested in the assay buffer containing 20 mM HEPES pH 8.5, 100 mM NaCl, and 2.5% DMSO. The filter was set at ROX with no quencher and a passive filter. The protein melting temperature (T_m) was calculated with fluorescence raw data by the Protein Thermal Shift software ver. 1.3 (Life Technologies). Data were plotted using GraphPad Prism 7.

Protein Crystallography and Data Collection and Processing. Purified BPTF_{2914–3037} was concentrated to 5 mg mL⁻¹ and crystallized at 16 °C using the sitting-drop vapor-diffusion method with a reservoir solution containing 200 mM lithium sulfate monohydrate, 100 mM Tris pH 8.5, and 25% w/v polyethylene glycol 3350. The crystals were soaked with 2 mM solutions of the indicated compounds (in a reservoir solution with 1% DMSO) for five days and were subsequently flash-cooled in liquid nitrogen for data collection with 15% glycerol (v/v). X-ray diffraction data were collected at beamlines BL17U1 and BL19U1 in the Shanghai Synchrotron Radiation Facility (SSRF). All data sets, which were processed with HKL-3000, are summarized in Table S2. Raw data was further processed using the HKL program suite, and the initial models were solved by molecular replacement with the PDB entry 3QTZ as the search template. Then, the initial structure was rebuilt using the AutoBuild³⁵ module of Phenix. Ligands were fit to the electron density map with the LigandFit³⁶ module of Phenix and Coot.³⁷ Then, complex structures were refined for several rounds using Phenix. Structure validation was performed using MolProbity.³⁸

Surface Plasma Resonance (SPR). A Biacore T200 instrument (GE Healthcare) was used to analyze the binding interactions with a direct binding assay format. The purified protein was immobilized on a CM5 sensor chip at the concentration of 50 μg mL⁻¹. The system was equilibrated by HBS buffer (25 mM HEPES pH 8.0, 150 mM NaCl, and 0.05% (v/v) P20 surfactant) containing 0.2% (v/v) DMSO. Compounds were diluted in the HBS buffer at the indicated concentration. Samples were injected over the protein and reference surfaces for 30 s and included a 120 s dissociation time. Data analysis was conducted via the state and binding model of the T200 evaluation software (GE Healthcare). Data were fitted globally using Biacore T200 Evaluation software to determine the binding kinetic rate constants, k_a (M⁻¹ s⁻¹) and k_d (s⁻¹), and the equilibrium dissociation constant K_D (M).

AlphaScreen. The selectivity against the BRD-family proteins, including BRD2(1), BRD2(2), BRD4(1), BRD4(2), p300-BRD, CBP-BRD, and SMARCA2-BRD, was determined by an Alpha Screen assay. In a 384-well plate, 12.5 nM BRD2(1) and 25 nM acetylated H4, 100 nM BRD2(2) and 75 nM acetylated H4, 12.5 nM BRD4(1) and 25 nM acetylated H4, 25 nM BRD4(2) and 50 nM acetylated H4, 40 nM p300-BRD and 100 nM acetylated H4, 20 nM CBP-BRD and 200 nM acetylated H4, and 100 nM SMARCA2-BRD and 100 nM acetylated H4 were mixed and incubated for 1 h. Then, 10 μL beads were added, and the plate was incubated for another 1 h before signal collection.

Cell Culture and Cell Viability Assay. The MLL-rearranged leukemia cell line of MV-4-11 and human normal cell lines (HUV-EC-C and MRC-5) were purchased from American Type Culture Collection (ATCC) and were cultured in either RPMI-1640 or DMEM medium (Gibco) supplemented with 10% FBS and 1% penicillin/streptomycin, maintained in a humidified incubator (37 °C, 5% CO₂), and checked regularly for mycoplasma contamination. Cells (5000–10 000 cells, 100 μL per well) were dispensed into 96-well microplates (Corning, no. 3599) in triplicate and incubated for 10 h in a humidified incubator. Subsequently, cells were treated with the indicated serial dilutions of the compounds or DMSO for five days. Cell viability was assessed using a CellTiter-Glo Kit (10 μL per well, Promega). Luminescence curves, which were recorded by an Envision Reader, were fit using the nonlinear fit module (four parameters, log dose versus response) to determine IC₅₀ values in GraphPad Prism 7.

Quantitative Real-Time PCR. MV-4-11 cells were seeded in 6-well plates (8 × 10⁵ cells/well) in the RPMI-1640 medium overnight before drug treatment. Cells were treated with either compounds or DMSO for 12 h. Total RNA was extracted using a TRIzol reagent (Vazyme, R401–01) following the manufacturer's instructions and

was reverse transcribed to cDNA with HiScript II Q Select RT SuperMix (Vazyme, R232–01). Real-time PCR analysis was performed in the QuantStudio 6 Flex Real-Time PCR system using the ChamQ SYBR qPCR master mix (Vazyme, Q331–02, low ROX premixed). The GAPDH gene was used as a normalization control for the gene expression levels. Primer sequences are listed in Table S1.

Cell Cycle and Apoptosis Analysis. MV-4–11 cells were treated with the indicated compounds or a DMSO control for 24 h before being harvested by centrifugation and washed twice with ice-cold PBS. For cell cycle detection, cells were fixed with ice-cold 70% ethanol overnight, resuspended with a cell cycle staining solution and RNase A, and diluted in PBS (Yeasen, no. 40301ES50). For the apoptosis analysis, cells were resuspended in 400 μL of the binding buffer and incubated with 5 μL of FITC Annexin V and propidium iodide for 30 min at 37 °C in the dark. Cell cycle and apoptosis data were acquired by flow cytometry on BD FACS Aria.

Western Blotting. Cell lysate samples were heated in a 95 °C heat block for 20 min and separated by 12% acrylamide SDS-PAGE in a Tris-glycine buffer. The proteins were transferred to nitrocellulose membranes (GE Healthcare) and blocked for 1 h at room temperature in 5% nonfat milk (diluted in TBST). Blots were incubated with shaking at 4 °C overnight with the following primary antibodies: c-Myc (Cell Signaling Technology, catalog no. 18583) and GAPDH (Cell Signaling Technology, no. 5174). After the incubation of primary antibodies, blots were incubated with a 1:10 000 dilution of the secondary antibody (BBI life, catalog no. D110058) for 1 h at room temperature. Images were detected by a GE ImageQuant LAS 4000 system with SuperSignal WestDura (Thermo Scientific, no. 34076) as the HRP substrate.

NanoBRET. Halo-tagged Histone H4 and NanoLuc-tagged BPTF-BRD plasmids were constructed, and NanoBRET assays were performed according to the manufacturer instructions (Promega). To elevate the assay window, 2.5 μM SAHA was added to the mixture.

■ ASSOCIATED CONTENT

Supporting Information

The Supporting Information is available free of charge at <https://pubs.acs.org/doi/10.1021/acs.jmedchem.1c00721>.

Dose dependent inhibitory activities of DC-BPi-04–17, NMR spectra of BPTF-BRD binding with DC-BPi-11, structural comparison of other bromodomain family members with BPTF-BRD, compound effect on the proliferation of normal human endothelial cells, primer sequences, X-ray crystallography data collection and refinement statistics, NMR data, and purity data (PDF)

Compound molecular formula strings (CSV)

BPTF-BRD in complex with DC-BPi-03 (CIF)

BPTF-BRD in complex with DC-BPi-07 (CIF)

BPTF-BRD in complex with DC-BPi-11 (CIF)

Accession Codes

Atomic coordinates for the X-ray structures of BPTF-BRD in complex with DC-BPi-03, DC-BPi-07, and DC-BPi-11 have been deposited in the Protein Data Bank (PDB IDs 7F5D, 7F5C, and 7F5E, respectively) and will be released upon publication.

■ AUTHOR INFORMATION

Corresponding Authors

Wenchao Lu – Stanford Cancer Institute, Stanford School of Medicine, Stanford University, Stanford, California 94305, United States; orcid.org/0000-0003-1175-365X; Email: wclu@stanford.edu

Hua Lin – The Chemical Biology Center, Drug Design and Discovery Center, State Key Laboratory of Drug Research,

Shanghai Institute of Materia Medica, Chinese Academy of Sciences, Shanghai 201203, China; Biomedical Research Center of South China, College of Life Sciences, Fujian Normal University, Fuzhou 350117, China; orcid.org/0000-0002-0840-6553; Email: hlin@fjnu.edu.cn

Cheng Luo – School of Pharmacy, Fujian Medical University, Fuzhou 350122, China; School of Chinese Materia Medica, Nanjing University of Chinese Medicine, Nanjing 210023, China; School of Pharmacy, Fudan University, Shanghai 201203, China; The Chemical Biology Center, Drug Design and Discovery Center, State Key Laboratory of Drug Research, Shanghai Institute of Materia Medica, Chinese Academy of Sciences, Shanghai 201203, China; orcid.org/0000-0003-3864-8382; Email: cluo@simm.ac.cn

Authors

Tian Lu – School of Pharmacy, Fujian Medical University, Fuzhou 350122, China; Guizhou University of Traditional Chinese Medicine, Guiyang, Guizhou 550025, China; School of Chinese Materia Medica, Nanjing University of Chinese Medicine, Nanjing 210023, China

Haibo Lu – School of Pharmacy, Fudan University, Shanghai 201203, China; The Chemical Biology Center, Drug Design and Discovery Center, State Key Laboratory of Drug Research, Shanghai Institute of Materia Medica, Chinese Academy of Sciences, Shanghai 201203, China

Zhe Duan – The Chemical Biology Center, Drug Design and Discovery Center, State Key Laboratory of Drug Research, Shanghai Institute of Materia Medica, Chinese Academy of Sciences, Shanghai 201203, China; School of Pharmacy, Nanchang University, Nanchang 330006, China

Jun Wang – The Chemical Biology Center, Drug Design and Discovery Center, State Key Laboratory of Drug Research, Shanghai Institute of Materia Medica, Chinese Academy of Sciences, Shanghai 201203, China

Jie Han – The Chemical Biology Center, Drug Design and Discovery Center, State Key Laboratory of Drug Research, Shanghai Institute of Materia Medica, Chinese Academy of Sciences, Shanghai 201203, China

Senhao Xiao – The Chemical Biology Center, Drug Design and Discovery Center, State Key Laboratory of Drug Research, Shanghai Institute of Materia Medica, Chinese Academy of Sciences, Shanghai 201203, China

HuanHuan Chen – Laboratory of Pharmaceutical Analysis, Shanghai Institute of Materia Medica, Chinese Academy of Sciences, Shanghai 201203, China

Hao Jiang – The Chemical Biology Center, Drug Design and Discovery Center, State Key Laboratory of Drug Research, Shanghai Institute of Materia Medica, Chinese Academy of Sciences, Shanghai 201203, China

Yu Chen – The Chemical Biology Center, Drug Design and Discovery Center, State Key Laboratory of Drug Research, Shanghai Institute of Materia Medica, Chinese Academy of Sciences, Shanghai 201203, China

Feng Yang – The Chemical Biology Center, Drug Design and Discovery Center, State Key Laboratory of Drug Research, Shanghai Institute of Materia Medica, Chinese Academy of Sciences, Shanghai 201203, China

Qi Li – The Chemical Biology Center, Drug Design and Discovery Center, State Key Laboratory of Drug Research, Shanghai Institute of Materia Medica, Chinese Academy of Sciences, Shanghai 201203, China

Dongying Chen – Laboratory of Pharmaceutical Analysis, Shanghai Institute of Materia Medica, Chinese Academy of Sciences, Shanghai 201203, China

Jin Lin – School of Pharmacy, Fujian Medical University, Fuzhou 350122, China

Bo Li – The Chemical Biology Center, Drug Design and Discovery Center, State Key Laboratory of Drug Research, Shanghai Institute of Materia Medica, Chinese Academy of Sciences, Shanghai 201203, China; orcid.org/0000-0002-4279-4596

Hualiang Jiang – The Chemical Biology Center, Drug Design and Discovery Center, State Key Laboratory of Drug Research, Shanghai Institute of Materia Medica, Chinese Academy of Sciences, Shanghai 201203, China

Kaixian Chen – School of Chinese Materia Medica, Nanjing University of Chinese Medicine, Nanjing 210023, China; The Chemical Biology Center, Drug Design and Discovery Center, State Key Laboratory of Drug Research, Shanghai Institute of Materia Medica, Chinese Academy of Sciences, Shanghai 201203, China

Complete contact information is available at:
<https://pubs.acs.org/10.1021/acs.jmedchem.1c00721>

Author Contributions

[†]T.L., H.L., and Z.D. are co-first authors and contributed equally to this work.

Notes

The authors declare no competing financial interest.

ACKNOWLEDGMENTS

We thank the staff of the BL17UB and BL19U1 beamlines at the National Protein Science Facility (NFPS) in the Shanghai Synchrotron Radiation Facility for their assistance during the data collection process. We are very grateful for the instrumental support and technical support of the Shanghai National Protein Science Center (Shanghai Science Research Center Protein Expression and Purification System). We gratefully acknowledge financial support from the National Natural Science Foundation of China (81625022, 91853205, and 81821005 to C.L. and 21820102008 to H.J.); the Science and Technology Commission of Shanghai Municipality (18431907100 to H.J., Y811298033 to Q.L., and 19XD1404700 to C.L.); and the scientific research innovation program “Xiyuanjiang River Scholarship” of the College of Life Sciences, Fujian Normal University, the State Key Laboratory of Drug Research (SIMM2105KF-07 to H.L.).

ABBREVIATIONS USED

BET, bromodomain and extra C-terminal domain; BPTF, bromodomain PHD finger transcription factor; BRD, bromodomain; BRD2, bromodomain-containing protein 2; BRD4, bromodomain-containing protein 4; CBP, cyclic adenosine monophosphate response element binding protein binding protein; DCM, dichloromethane; DMF, dimethylformamide; DMSO, dimethyl sulfoxide; Et₃N, trimethylamine; EtOAc, ethyl acetate; HTRF, homogeneous time-resolved fluorescence; NMR, nuclear magnetic resonance; RT-PCR, reverse transcription-polymerase chain reaction; SAR, structure–activity relationship; SGC, structural genomics consortium; SMARCA2, SWI/SNF-related matrix-associated actin-dependent regulator of chromatin, subfamily A, member 2; SPR, surface plasmon resonance; THF, tetrahydrofuran

REFERENCES

- (1) Ruthenburg, A. J.; Li, H.; Milne, T. A.; Dewell, S.; McGinty, R. K.; Yuen, M.; Ueberheide, B.; Dou, Y.; Muir, T. W.; Patel, D. J.; Allis, C. D. Recognition of a mononucleosomal histone modification pattern by bptf via multivalent interactions. *Cell* **2011**, *145*, 692–706.
- (2) Dar, A. A.; Nosrati, M.; Bezrookove, V.; de Semir, D.; Majid, S.; Thummala, S.; Sun, V.; Tong, S.; Leong, S. P.; Minor, D.; Billings, P. R.; Soroceanu, L.; Debs, R.; Miller, J. R., 3rd; Sagebiel, R. W.; Kashani-Sabet, M. The role of BPTF in melanoma progression and in response to braf-targeted therapy. *J. Natl. Cancer Inst* **2015**, *107*, djv034.
- (3) Li, H.; Ilin, S.; Wang, W.; Duncan, E. M.; Wysocka, J.; Allis, C. D.; Patel, D. J. Molecular basis for site-specific read-out of histone h3k4me3 by the bptf phd finger of nurf. *Nature* **2006**, *442*, 91–95.
- (4) Jones, M. H.; Hamana, N.; Shimane, M. Identification and characterization of bptf, a novel bromodomain transcription factor. *Genomics* **2000**, *63*, 35–39.
- (5) Richart, L.; Real, F. X.; Sanchez-Arevalo Lobo, V. J. C-myc partners with bptf in human cancer. *Mol. Cell Oncol* **2016**, *3*, e1152346.
- (6) Jordan-Sciutto, K. L.; Dragich, J. M.; Bowser, R. DNA binding activity of the fetal alz-50 clone 1 (fac1) protein is enhanced by phosphorylation. *Biochem. Biophys. Res. Commun.* **1999**, *260*, 785–789.
- (7) Frey, W. D.; Chaudhry, A.; Slepicka, P. F.; Ouellette, A. M.; Kirberger, S. E.; Pomerantz, W. C. K.; Hannon, G. J.; Dos Santos, C. O. Bptf maintains chromatin accessibility and the self-renewal capacity of mammary gland stem cells. *Stem Cell Rep.* **2017**, *9*, 23–31.
- (8) Goller, T.; Vauti, F.; Ramasamy, S.; Arnold, H. H. Transcriptional regulator bptf/fac1 is essential for trophoblast differentiation during early mouse development. *Mol. Cell. Biol.* **2008**, *28*, 6819–6827.
- (9) Jain, A. K.; Barton, M. C. Bromodomain histone readers and cancer. *J. Mol. Biol.* **2017**, *429*, 2003–2010.
- (10) Dar, A. A.; Majid, S.; Bezrookove, V.; Phan, B.; Ursu, S.; Nosrati, M.; De Semir, D.; Sagebiel, R. W.; Miller, J. R., 3rd; Debs, R.; Cleaver, J. E.; Kashani-Sabet, M. Bptf transduces mitf-driven prosurvival signals in melanoma cells. *Proc. Natl. Acad. Sci. U. S. A.* **2016**, *113*, 6254–6258.
- (11) Buganim, Y.; Goldstein, I.; Lipson, D.; Milyavsky, M.; Polak-Charcon, S.; Mardouk, C.; Solomon, H.; Kalo, E.; Madar, S.; Brosh, R.; Perelman, M.; Navon, R.; Goldfinger, N.; Barshack, I.; Yakhini, Z.; Rotter, V. A novel translocation breakpoint within the bptf gene is associated with a pre-malignant phenotype. *PLoS One* **2010**, *5*, e9657.
- (12) Xiao, S.; Liu, L.; Lu, X.; Long, J.; Zhou, X.; Fang, M. The prognostic significance of bromodomain phd-finger transcription factor in colorectal carcinoma and association with vimentin and e-cadherin. *J. Cancer Res. Clin. Oncol.* **2015**, *141*, 1465–1474.
- (13) Kim, K.; Punj, V.; Choi, J.; Heo, K.; Kim, J. M.; Laird, P. W.; An, W. Gene dysregulation by histone variant h2a.Z in bladder cancer. *Epigenet. Chromatin* **2013**, *6*, 34.
- (14) Richart, L.; Carrillo-de Santa Pau, E.; Rio-Machin, A.; de Andres, M. P.; Cigudosa, J. C.; Lobo, V. J. S.; Real, F. X. Bptf is required for c-MYC transcriptional activity and in vivo tumorigenesis. *Nat. Commun.* **2016**, *7*, 10153.
- (15) Morrison, E. A.; Bowerman, S.; Sylvers, K. L.; Wereszczynski, J.; Musselman, C. A. The conformation of the histone h3 tail inhibits association of the bptf phd finger with the nucleosome. *eLife* **2018**, *7*, e31481.
- (16) Zhan, W.; Liao, X.; Wang, Y.; Li, L.; Li, J.; Chen, Z.; Tian, T.; He, J. Circctc1 promotes the self-renewal of colon tics through bptf-dependent c-myc expression. *Carcinogenesis* **2019**, *40*, S60–S68.
- (17) Wu, B.; Wang, Y.; Wang, C.; Wang, G. G.; Wu, J.; Wan, Y. Y. Bptf is essential for t cell homeostasis and function. *J. Immunol.* **2016**, *197*, 4325–4333.
- (18) Amorim, S.; Stathis, A.; Gleeson, M.; Iyengar, S.; Magarotto, V.; Leleu, X.; Morschhauser, F.; Karlin, L.; Broussais, F.; Rezai, K.; Herait, P.; Kahatt, C.; Lokiec, F.; Salles, G.; Facon, T.; Palumbo, A.; Cunningham, D.; Zucca, E.; Thieblemont, C. Bromodomain inhibitor otx015 in patients with lymphoma or multiple myeloma: A dose-escalation, open-label, pharmacokinetic, phase 1 study. *Lancet Haematol* **2016**, *3*, e196–204.
- (19) Filippakopoulos, P.; Qi, J.; Picaud, S.; Shen, Y.; Smith, W. B.; Fedorov, O.; Morse, E. M.; Keates, T.; Hickman, T. T.; Felletar, I.; Philpott, M.; Munro, S.; McKeown, M. R.; Wang, Y.; Christie, A. L.; West, N.; Cameron, M. J.; Schwartz, B.; Heightman, T. D.; La Thangue, N.; French, C. A.; Wiest, O.; Kung, A. L.; Knapp, S.; Bradner, J. E. Selective inhibition of bet bromodomains. *Nature* **2010**, *468*, 1067–1073.
- (20) Faivre, E. J.; McDaniel, K. F.; Albert, D. H.; Mantena, S. R.; Plotnik, J. P.; Wilcox, D.; Zhang, L.; Bui, M. H.; Sheppard, G. S.; Wang, L.; Sehgal, V.; Lin, X.; Huang, X.; Lu, X.; Uziel, T.; Hessler, P.; Lam, L. T.; Bellin, R. J.; Mehta, G.; Fidanze, S.; Pratt, J. K.; Liu, D.; Hasvold, L. A.; Sun, C.; Panchal, S. C.; Nicolette, J. J.; Fossey, S. L.; Park, C. H.; Longenecker, K.; Bigelow, L.; Torrent, M.; Rosenberg, S. H.; Kati, W. M.; Shen, Y. Selective inhibition of the bd2 bromodomain of bet proteins in prostate cancer. *Nature* **2020**, *578*, 306–310.
- (21) McDaniel, K. F.; Wang, L.; Soltwedel, T.; Fidanze, S. D.; Hasvold, L. A.; Liu, D.; Mantei, R. A.; Pratt, J. K.; Sheppard, G. S.; Bui, M. H.; Faivre, E. J.; Huang, X.; Li, L.; Lin, X.; Wang, R.; Warder, S. E.; Wilcox, D.; Albert, D. H.; Magoc, T. J.; Rajaraman, G.; Park, C. H.; Hutchins, C. W.; Shen, J. J.; Edalji, R. P.; Sun, C. C.; Martin, R.; Gao, W.; Wong, S.; Fang, G.; Elmore, S. W.; Shen, Y.; Kati, W. M. Discovery of n-(4-(2,4-difluorophenoxy)-3-(6-methyl-7-oxo-6,7-dihydro-1h-pyrrolo[2,3-c]pyridin-4-yl)phenyl)ethanesulfonamide (abbv-075/mivebresib), a potent and orally available bromodomain and extraterminal domain (bet) family bromodomain inhibitor. *J. Med. Chem.* **2017**, *60*, 8369–8384.
- (22) Bernasconi, E.; Gaudio, E.; Lejeune, P.; Tarantelli, C.; Cascione, L.; Kwee, I.; Spriano, F.; Rinaldi, A.; Mensah, A. A.; Chung, E.; Stathis, A.; Siegel, S.; Schmees, N.; Ocker, M.; Zucca, E.; Haendler, B.; Bertoni, F. Preclinical evaluation of the bet bromodomain inhibitor bay 1238097 for the treatment of lymphoma. *Br. J. Haematol.* **2017**, *178*, 936–948.
- (23) Tanaka, M.; Roberts, J. M.; Qi, J.; Bradner, J. E. Inhibitors of emerging epigenetic targets for cancer therapy: A patent review (2010–2014). *Pharm. Pat. Anal.* **2015**, *4*, 261–284.
- (24) Welti, J.; Sharp, A.; Brooks, N.; Yuan, W.; McNair, C.; Chand, S. N.; Pal, A.; Figueiredo, I.; Riisnaes, R.; Gurel, B.; Rekowski, J.; Bogdan, D.; West, W.; Young, B.; Raja, M.; Prosser, A.; Lane, J.; Thomson, S.; Worthington, J.; Onions, S.; Shannon, J.; Paoletta, S.; Brown, R.; Smyth, D.; Harbottle, G. W.; Gil, V. S.; Miranda, S.; Crespo, M.; Ferreira, A.; Pereira, R.; Tunariu, N.; Carreira, S.; Neeb, A. J.; Ning, J.; Swain, A.; Taddei, D.; Schiewer, M. J.; Knudsen, K. E.; Pegg, N.; de Bono, J. S. Targeting p300/cbp axis in lethal prostate cancer. *Cancer Discovery* **2021**, *11*, 1118.
- (25) Urick, A. K.; Hawk, L. M.; Cassel, M. K.; Mishra, N. K.; Liu, S.; Adhikari, N.; Zhang, W.; dos Santos, C. O.; Hall, J. L.; Pomerantz, W. C. Dual screening of bptf and brd4 using protein-observed fluorine nmr uncovers new bromodomain probe molecules. *ACS Chem. Biol.* **2015**, *10*, 2246–2256.
- (26) Kirberger, S. E.; Ycas, P. D.; Johnson, J. A.; Chen, C.; Ciccone, M. F.; Woo, R. W. L.; Urick, A. K.; Zahid, H.; Shi, K.; Aihara, H.; McAllister, S. D.; Kashani-Sabet, M.; Shi, J.; Dickson, A.; Dos Santos, C. O.; Pomerantz, W. C. K. Selectivity, ligand deconstruction, and cellular activity analysis of a bptf bromodomain inhibitor. *Org. Biomol. Chem.* **2019**, *17*, 2020–2027.
- (27) Picaud, S.; Leonards, K.; Lambert, J. P.; Dovey, O.; Wells, C.; Fedorov, O.; Monteiro, O.; Fujisawa, T.; Wang, C. Y.; Lingard, H.; Tallant, C.; Nikbin, N.; Guetzoyan, L.; Ingham, R.; Ley, S. V.; Brennan, P.; Muller, S.; Samsonova, A.; Gingras, A. C.; Schwaller, J.; Vassiliou, G.; Knapp, S.; Filippakopoulos, P. Promiscuous targeting of bromodomains by bromosporine identifies bet proteins as master regulators of primary transcription response in leukemia. *Sci. Adv.* **2016**, *2*, e1600760.
- (28) Humphreys, P. G.; Bamborough, P.; Chung, C. W.; Craggs, P. D.; Gordon, L.; Grandi, P.; Hayhow, T. G.; Hussain, J.; Jones, K. L.

Lindon, M.; Michon, A. M.; Renaux, J. F.; Suckling, C. J.; Tough, D. F.; Prinjha, R. K. Discovery of a potent, cell penetrant, and selective p300/cbp-associated factor (pcaf)/general control nonderepressible 5 (gcn5) bromodomain chemical probe. *J. Med. Chem.* **2017**, *60*, 695–709.

(29) Zhang, D.; Han, J.; Lu, W.; Lian, F.; Wang, J.; Lu, T.; Tao, H.; Xiao, S.; Zhang, F.; Liu, Y. C.; Liu, R.; Zhang, N.; Jiang, H.; Chen, K.; Zhao, C.; Luo, C. Discovery of alkoxy benzamide derivatives as novel bptf bromodomain inhibitors via structure-based virtual screening. *Bioorg. Chem.* **2019**, *86*, 494–500.

(30) Ycas, P. D.; Zahid, H.; Chan, A.; Olson, N. M.; Johnson, J. A.; Talluri, S. K.; Schonbrunn, E.; Pomerantz, W. C. K. New inhibitors for the bptf bromodomain enabled by structural biology and biophysical assay development. *Org. Biomol. Chem.* **2020**, *18*, 5174–5182.

(31) Roussy, M.; Bilodeau, M.; Jouan, L.; Tibout, P.; Laramee, L.; Lemyre, E.; Leveille, F.; Tihy, F.; Cardin, S.; Sauvageau, C.; Couture, F.; Louis, I.; Choblet, A.; Patey, N.; Gendron, P.; Duval, M.; Teira, P.; Hebert, J.; Wilhelm, B. T.; Choi, J. K.; Gruber, T. A.; Bittencourt, H.; Cellot, S. Nup98-bptf gene fusion identified in primary refractory acute megakaryoblastic leukemia of infancy. *Genes, Chromosomes Cancer* **2018**, *57*, 311–319.

(32) Gong, Y.-C.; Liu, D.-C.; Li, X.-P.; Dai, S.-P. Bptf biomarker correlates with poor survival in human nscl. *Eur. Rev. Med. Pharmacol Sci.* **2017**, *21*, 102–107.

(33) Wang, Y.; Li, L.; Zhang, B.; Xing, J.; Chen, S.; Wan, W.; Song, Y.; Jiang, H.; Jiang, H.; Luo, C.; Zheng, M. Discovery of novel disruptor of silencing telomeric 1-like (dot1l) inhibitors using a target-specific scoring function for the (s)-adenosyl-l-methionine (sam)-dependent methyltransferase family. *J. Med. Chem.* **2017**, *60*, 2026–2036.

(34) Pan, L.; Tang, Z.; Pan, L.; Tang, R. MicroRNA-3666 inhibits lung cancer cell proliferation, migration, and invasiveness by targeting bptf. *Biochem. Cell Biol.* **2019**, *97*, 415–422.

(35) Terwilliger, T. C.; Grosse-Kunstleve, R. W.; Afonine, P. V.; Moriarty, N. W.; Zwart, P. H.; Hung, L.-W.; Read, R. J.; Adams, P. D. Iterative model building, structure refinement and density modification with the phenix autobuild wizard. *Acta Crystallogr., Sect. D: Biol. Crystallogr.* **2008**, *64*, 61–69.

(36) Terwilliger, T. C.; Klei, H.; Adams, P. D.; Moriarty, N. W.; Cohn, J. D. Automated ligand fitting by core-fragment fitting and extension into density. *Acta Crystallogr., Sect. D: Biol. Crystallogr.* **2006**, *62*, 915–922.

(37) Emsley, P.; Lohkamp, B.; Scott, W. G.; Cowtan, K. Features and development of coot. *Acta Crystallogr., Sect. D: Biol. Crystallogr.* **2010**, *66*, 486–501.

(38) Chen, V. B.; Arendall, W. B.; Headd, J. J.; Keedy, D. A.; Immormino, R. M.; Kapral, G. J.; Murray, L. W.; Richardson, J. S.; Richardson, D. C. Molprobity: All-atom structure validation for macromolecular crystallography. *Acta Crystallogr., Sect. D: Biol. Crystallogr.* **2010**, *66*, 12–21.